# Structure and Geochronology of the Alpine Schist, New Zealand

Thesis submitted in accordance with the requirements of the University of Adelaide for an Honours Degree in Geology

William Hagger

November 2013


THE UNIVERSITY of ADELAIDE

# STRUCTURE AND GEOCHRONOLOGY OF THE ALPINE SCHIST, NEW ZEALAND

## STRUCTURE AND AGE OF THE ALPINE SCHIST FABRICS


## ABSTRACT

The Alpine Schist is located on the eastern margin of the Alpine Fault, which accommodates oblique collision between the Pacific and Australian plates in New Zealand. Collision has been active since the Cenozoic and exhumation models predict that surface rocks were buried ~20km in the Pliocene. Despite this, fabrics of Mesozoic age are inferred to be preserved at the surface. In order to test the age of fabric formation, transects were conducted across the Alpine Schist to measure the foliation. Rock samples were collected to date the age of zircon and $^{40}Ar/^{39}Ar$ age of muscovite in order to constrain the age of metamorphism and fabric formation within the Alpine Schist. The structural data displayed two populations of foliations: a dominant foliation tracking towards the orientation of the Alpine Fault and a minor shallower orientation. The geochronological data highlighted ages for the formation and deposition of the Alpine Schist protolith and metamorphism associated with the Rangitata Orogeny. Muscovite $^{40}Ar/^{39}Ar$ data analysis yielded Pleistocene closure temperatures of the argon system. The heterogeneous foliation orientation and muscovite age suggested differential strain and fabric formation with the Alpine Schist during Plesitocene uplift along the Alpine Fault. The study of the active Southern Alps orogen and constraining the structural and geochronological features will enable more accurate interpretation of fossil orogens and their relationship with plate tectonics.



## KEYWORDS

Geochronology, Structural, Alpine Schist, New Zealand, Southern Alps, Zircon, Muscovite

## Contents

List of Figures and Tables

## INTRODUCTION

Dating of fabrics in terranes with complex metamorphic histories presents many challenges. A complex tectonic history is preserved within the Alpine Schist, beginning with the Rangitata Orogeny (~190-80 Ma) (Grapes 1995), which involved Cretaceous crustal thickening from collision between the Australian and Pacific Plates (Vry et al. 2008). The Miocene-Present Kaikoura orogeny resulted from increasingly oblique collision between the Australian and Pacific Plates from ~10 Ma. Current uplift rates are estimated at ~6-9 mm/yr (Little et al. 2005). The Alpine Schist lies directly above the Alpine Fault, the plate boundary between the Australian and Pacific Plates. The Alpine Schist is progressively metamorphosed to higher grades towards the Alpine Fault. Although the fault itself is largely a Neogene structure (Cooper et al. 1987), fabrics within the Alpine Schist are commonly interpreted to be Mesozoic (Vry et al. 2008). Despite agreement that during the Cenozoic period of rapid convergence, over 25 km of uplift occurred (Grapes 1995). At similar depths, rocks would be at conditions sufficient to produce the metamorphic assemblages and fabric seen in the Alpine Schist. Therefore, I propose that the Alpine Schist fabrics are Pliocene to recent and result from active metamorphism during uplift of the Alpine Schist. I shall test this by examining the ages of zircons from the Alpine Schist, focussing particularly on rim domains, investigating muscovite $^{40}Ar/^{39}Ar$ age data and combining these results with structural transects in the region to determine whether there is evidence of Pliocene and younger fabric formation.

## GEOLOGICAL SETTING

The Alpine Schist is a unit within the Haast Schist Belt of New Zealand. It is present as a steeply dipping and narrow (~10-20 km wide) belt (Vry et al. 2004) of metamorphosed greywacke and argillite (Vry et al. 2008). The Alpine Schist is present on the eastern side of

the Alpine Fault (Figure 1b). The schist grades from the garnet-oligoclase mylonite zone of the Alpine Schist easterly across mineral isograds to a garnet and biotite zone then into the chlorite transitional zone into the Otago Schist (Grapes 1995). This transfer, west to east, moves from amphibolites facies to lower greenschist facies (Little et al. 2002, Grapes 1995). Variation of grade and mineral isograds along the strike of the schist belt are attributed to folding during Oligocene-Miocene tectonism (Mortimer and Cooper 2004). Within 1-2 kilometres of the Alpine Fault the rock units are mylonitised (Sibson et al. 1981) (Fig 1c). The mylonitic units have foliation that dips ~25-60$^0$ to the Alpine Fault (Little et al. 2002).

The geological history of the Southern Alps and the Alpine Schist is complex. Sedimentary protolith deposition occurred in the Permian and Triassic (Vry et al. 2008). The tectonic history of the region began with the Rangitata Orogeny that generated ~10-14 km of uplift during the Mesozoic (Grapes 1995). The region underwent crustal thickening at ~86 Ma prior to the opening of the Tasman Sea that occurred between ~84-82 Ma (Mortimer and Cooper 2004). The higher grade mineral assemblages are suggested by Vry et al. (2008) to have formed during this Late Cretaceous event.

The oblique component of collision between the Australian and Pacific plates increased ~10 Ma, with the earliest rock uplift of the Southern Alps occurring from ~8-7 Ma and propagating north during the Kaikoura Orogeny (Vry et al. 2004). The current plate motion of the Australian Plate relative to the Pacific Plate is east-northeast. This motion has a parallel slip component between the plates of 35.5 mm/yr and a collisional component orthogonal to the plate boundary of 10 mm/yr (Norris and Cooper 2000). This movement has been accommodated along the Alpine Fault with rapid uplift ~6-9 mm/yr (Little et al. 2005). The plate boundary parallel component of motion results in dextral-reverse slip along the Alpine Fault, which strikes ~18-20$^0$ to the west of the plate motion vector. Late Cenozoic uplift amounted to an estimated total of 25 km during this later period of rapid convergence (Little

et al. 2002). The rapid exhumation has exposed the Alpine Schist of the Torlesse Terrane along the eastern margin of the Southern Alps (Grapes 1995). The exhumation of the higher grade mylonitic units of the Alpine Schist occurred from the Pliocene, ~3 Ma, with ductile deformation occurring during transport up the hanging wall of the Alpine Fault (Little et al. 2002).

The depth of deformation and fabric formation is related to the depth of the Brittle-Ductile Transition Zone (BDTZ) where greenschist facies temperatures are reflected (Shi et al. 1996). The BDTZ represents the physical limit of ductile fabric formation as proposed by Grapes (1995) and Mortimer (2000), that the Alpine Schist represent a lower temperature recrystallisation, ~400–280$^{o}$ C, superimposed on the moderate to high P/T ~600–700$^{o}$ C, ~11 kbar, Otago Schist (Mortimer and Cooper 2004, Toy et al. 2010).

The BDTZ was inferred at a depth of ~10 km beneath the Alpine Schist by Wannamaker et al. (2002), interpreting a crustal conductor at this depth from the Southern Alps magnetotelluric soundings of Ingham (1996), to represent liquid trapped at the BDTZ from prograde metamorphism. The migration of these fluids through fractures in the upper crust form the localised undeformed hydrothermal veining and fluid alteration of the Alpine Schist (Craw 1992).

Garnet Sm-Nd and Lu-Hf ages collected by Vry et al. (2004) combined with existing (Rb-Sr, $^{40}$Ar/$^{39}$Ar, U/Pb and Sm-Nd) ages of deformational fabrics demonstrated different ages of mineral growth, with some growth and fabric formation of Cenozoic age. Later fission track data and $^{40}$Ar/$^{39}$Ar data collected by Little et al. (2005) yielded ages younger than the onset of the Kaikoura Orogeny. The reset apatite fission-track ages in the Central Southern Alps are statistically indistinguishable from 0 Ma, reset zircon fission-track ages were <1 Ma, biotite and muscovite K/Ar cooling ages from around the Franz Josef area are <2 Ma (Little et al. 2005). These ages correspond to Pliocene age and younger uplift of the Alpine Schist from

temperatures >500$^{o}$ C (Little et al. 2002). While these ages indicate young recrystallisation or cooling, the fabric forming events could not be constrained between Cretaceous or Cenozoic events(Toy et al. 2010).

Studies on the ductile fabrics of the Alpine Schist by Little et al. (2002), interpreted changes in quartz microstructure to have occurred at the BDTZ with a late Cenozoic increment of strain. However, it could not be distinguished from these quartz microstructures if the Alpine foliation behaved as a passive marker or was an active surface tracking towards the principal plane of finite strain. Studies of the crystallographic preferred orientations of quartz within the fabrics of the Alpine Schist by Toy et al. (2008) indicated a younger weaker fabric developed in the higher levels of the crust away from the Alpine Fault, as at depth in the higher temperature environment strain was lower. It was inferred by Toy et al. (2008) that mylonitic foliation was reinforced by this later stage uppercrustal strain. The examination of foliations from east to west towards the Alpine Fault indicated that the trajectory of foliation in the Alpine Schist approaches parallel with the Alpine Fault (Little et al. 2002).

Despite the extensive geochronological data collected from the Alpine Schist and evidence of Late Cenozoic mineral formation, the age of the Alpine Schist fabric has proved difficult to differentiate between Mesozoic and Cenozoic events. The proximity of the Alpine Schist to the Alpine Fault that has accommodated rapid uplift since the Neogene (Cooper et al. 1987) combined with the similar structural orientation of the Alpine Schist to the Alpine Fault (Little et al. 2002) challenges the assumption that the fabrics are Mesozoic. An alternative hypothesis is that the fabrics were recrystallised in Pliocene-Recent times, during the Kaikouran Orogeny.

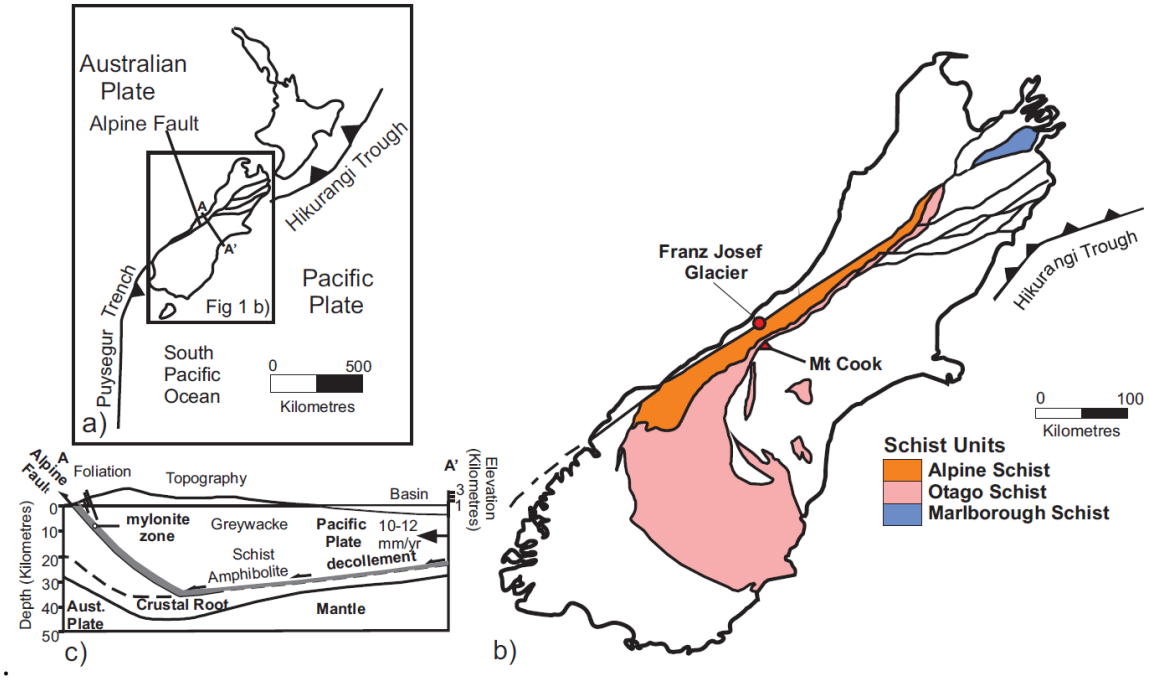


**Figure 1 (a) Regional map of the Pacific-Australian plate boundary in New Zealand showing the location of the Alpine Fault after Vry et al. (2004). (b) Schematic cross section A-A' across the Central Southern Alps near Franz Josef after Little et al. (2005). (c) Map of the South Island of New Zealand, showing schist units and reference locations after Vry et al. (2004).**

## METHODS

### Zircon textural investigation and U/Pb dating

Rock samples were selected from Alpine Schist units at the locations in Table 1, for U/Pb dating of zircons. Analysed samples were limited to those containing recoverable zircon grains.

**Table 1 GPS Locations of Rock Samples with recoverable zircon**

| Sample | GPS Coordinates | Lithology |
|---|---|---|
| NZ1309 | 43° 23' 15.9" S 170° 12'15.1" E | Mylonite |
| NZ1310 | 43° 23' 17.7" S 170° 12'32.5" E | Mylonite |
| NZ1315 | 43° 23' 15.9" S 170° 12'15.1" E | Mylonite |

The rocks were crushed, ground and sieved to create a fraction between 400 and 79 µm. The fraction was further separated using heavy liquids and magnetic methods, then handpicked under a binocular microscope to separate zircons. The zircons were mounted in an epoxy resin for analysis.

Zircon geochronology was undertaken using Laser Ablation Inductively Coupled Mass Spectrometry (LA-ICP-MS) following Payne et al. (2008), using a NEW Wave UP-213 laser attached to an Agilent 7500cx ICP-MS located at Adelaide Microscopy, The University of Adelaide. Cathodoluminescence and back scatter electron imaging of zircon were performed using a Phillips XL40 Scanning Electron Microscope located at Adelaide Microscopy, The University of Adelaide. Cathodoluminesence imaging was performed to determine zonation within the mounted zircon grains. The ablation was performed in a helium atmosphere with argon gas added immediately after the cell to aid the transport of material. The spot size for zircon analysis was 30 µm in diameter. The spot size was used to target the cores and textural domains of the zircon with maximum signal intensity for the mass spectrometer.

The frequency of the laser was 5 Hz and laser output percentage set at 55%, which resulted in average fluence of 2.26 J/cm$^2$ at the ablation site. A single analytical spot consisted of a 40 second gas blank followed by 80 seconds of data acquisition with the laser firing. The measured isotopes and their dwell times are shown in Table 2.

**Table 2 Measured Isotopes for zircon analyses**

| Isotope | Dwell Times |
|---|---|
| $^{204}$Pb | 10 ms |
| $^{206}$Pb | 15 ms |
| $^{207}$Pb | 30 ms |
| $^{238}$U | 15 ms |
| $^{208}$Pb | 10 ms |
| $^{232}$Th | 10ms |

The age calculations and mass bias were performed using the GLITTER software version 4.4.4 and the external primary standards, Plešovice, and primary zircon standard, GJ-1, after Jackson et al. (2004). The thermal mass ionization mass spectrometry derived normalization age for Plešovice and GJ-1 were assigned an overestimated uncertainty of 1%. Standard bracketing of every 10-20 unknowns and application of a linear correction were used to correct for instrument drift. The Thermal Ionisation Mass Spectrometry (TIMS), normalisation data for each isotopic system and standard can be seen in Table 3.

**Table 3 Published isotopic values of standards, GJ-1 (Jackson et al. 2004), Plešovice (Sláma et al. 2008)**

| Isotopic System | GJ-1 Age (Ma) | Plešovice Age (Ma) |
|---|---|---|
| $^{207}Pb/^{206}Pb$ | 607.7 ± 4.3 | 339.322 ± 0.25 |
| $^{206}Pb/^{238}U$ | 600.7 ± 1.1 | 337.13 ± 0.37 |
| $^{207}Pb/^{235}U$ | 602.0 ± 1.0 | 337.27 ± 0.11 |

Accuracy of the zircon methodology was verified by repeat analysis of the Plešovice standard. The weighted average ages for the isotopic system are seen in Table 4.

**Table 4 Isotopic System Weighted Averages**

| Isotopic System | GJ-1 Age (Ma) (n=62) | Plešovice Age (Ma) (n=15) |
|---|---|---|
| $^{207}Pb/^{206}Pb$ | 612.6 ± 41.1 | 380.1 ± 36.69 |
| $^{206}Pb/^{238}U$ | 599.8 ± 7.9 | 337.72 ± 4.454 |
| $^{207}Pb/^{235}U$ | 602.5 ± 9.2 | 343.95 ± 5.2 |

Data were rejected based on the presence of common lead using a combination of intensity of the raw $^{204}Pb$ counts. Following this, weighted average $^{207}Pb/^{206}Pb$ age calculations at 1σ are reported in the appendix, Supplementary Table 1.

## $^{40}Ar/^{39}Ar$ Dating Method

Fresh samples from the Alpine Schist mylonite zone were selected from 3 locations along an easterly transect away from the Alpine Fault, for coordinates, see Table 5. The samples were selected so that distance from the Alpine Fault could be correlated to any change in $^{40}Ar/^{39}Ar$ geochronological data.

**Table 5 Latitude and Longitude Coordinates of Muscovite Samples**

| Sample | GPS | Lithology |
|---|---|---|
| NZ1306 | 43° 23' 15.9" S 170° 12'15.1" E | Phyllite Schist |
| NZ1309 | 43° 23' 16.5" S 170° 12'18.8" E | Protomylonite |
| NZ1312 | 43° 23' 17.7" S 170° 12'32.5" E | Mylonite |

The samples were then crushed, sieved and magnetically separated with optically pure muscovite grains handpicked from the non-magnetic fraction using a binocular microscope. Following the $^{40}Ar/^{39}Ar$ methods of Jourdan and Renne (2007), the muscovites were prepared for irradiation at the Western Australian Argon Isotope Facility, operated by a consortium consisting of Curtin University and the University of Western Australia, then irradiated in the Hamilton McMaster University nuclear reactor (Canada) in position 5C along with the fluence monitor, Fish Canyon sanidine in each irradiation disc. The Fish Canyon sanidine has an adopted age of 28.305 ± 0.036 Ma (1σ) from work done by Renne et al. (2010), based on the calibration work of Jourdan and Renne (2007). The mean J-values computed from the standard grains within the small pits range from $0.00066100 \pm 0.99\times10^{-6}$ (0.15%) to $0.0066100 \pm 1.0\times10^{-6}$ (0.16%). These were used to determine the average and standard deviation of J-values of each irradiation disc. Mass discrimination was monitored using an automated air pipette and provided a mean value of 1.006286 ± 0.00342 per Dalton (Da),

relative to an air ratio of 298.56 ± 0.31 from the calculations of Lee et al. (2006). The correction factors for interfering isotopes are seen in Table 6.

**Table 6 Interfering Isotopes Correction Factors**

| Interfering Isotope System | Correction Factor |
|---|---|
| $(^{39}Ar/^{37}Ar)_{Ca}$ | 7.30x10-4 (±11%) |
| $(^{36}Ar/^{37}Ar)_{Ca}$ | 2.82x10-4 (± 1%) |
| $(^{40}Ar/^{39}Ar)_{K}$ | 6.76x10-4 (± 32%) |

Subsequent $^{40}Ar/^{39}Ar$ analyses were performed at the Western Australian Argon Isotope Facility at Curtin University. For the calculation of plateau ages at the 2σ level, Table 9 and Figure 11, the mean of all plateau steps was used with each step weighted by the inverse variance of the respective analytical error. The criteria for plateau identification requires at least 70% of $^{39}Ar$ distributed over a minimum of 3 consecutive steps with agreement at the 95% confidence interval and satisfying a p value of at least 0.05. A similar criteria is applied for the calculation of mini plateaus, except they include [50, 70]% $^{39}Ar$. All sources of error are included in the calculation.

## OBSERVATIONS AND RESULTS

### Structural Measurements and Sampling

Structural measurements were taken along four transects that lie roughly perpendicular to the Alpine Fault. Due to the thickness of Quaternary fluvio-glacial deposits and vegetation, transects were confined to outcrop along river channels. The transects can be seen in relation to the regional geology mapped by Cox and Barrell (2007) in Figure 2. The transect cross sections seen in Figure 3 were conducted along the Waiho River and its tributary, the Callery River, the Tatare Stream, Tommy Creek and along the Waikukupa River and its tributary, Hare Mare Creek. The dominant lithologies were a biotite-muscovite-quartz-feldspar phyllite and biotite-muscovite-garnet-quartz-feldspar mylonite.

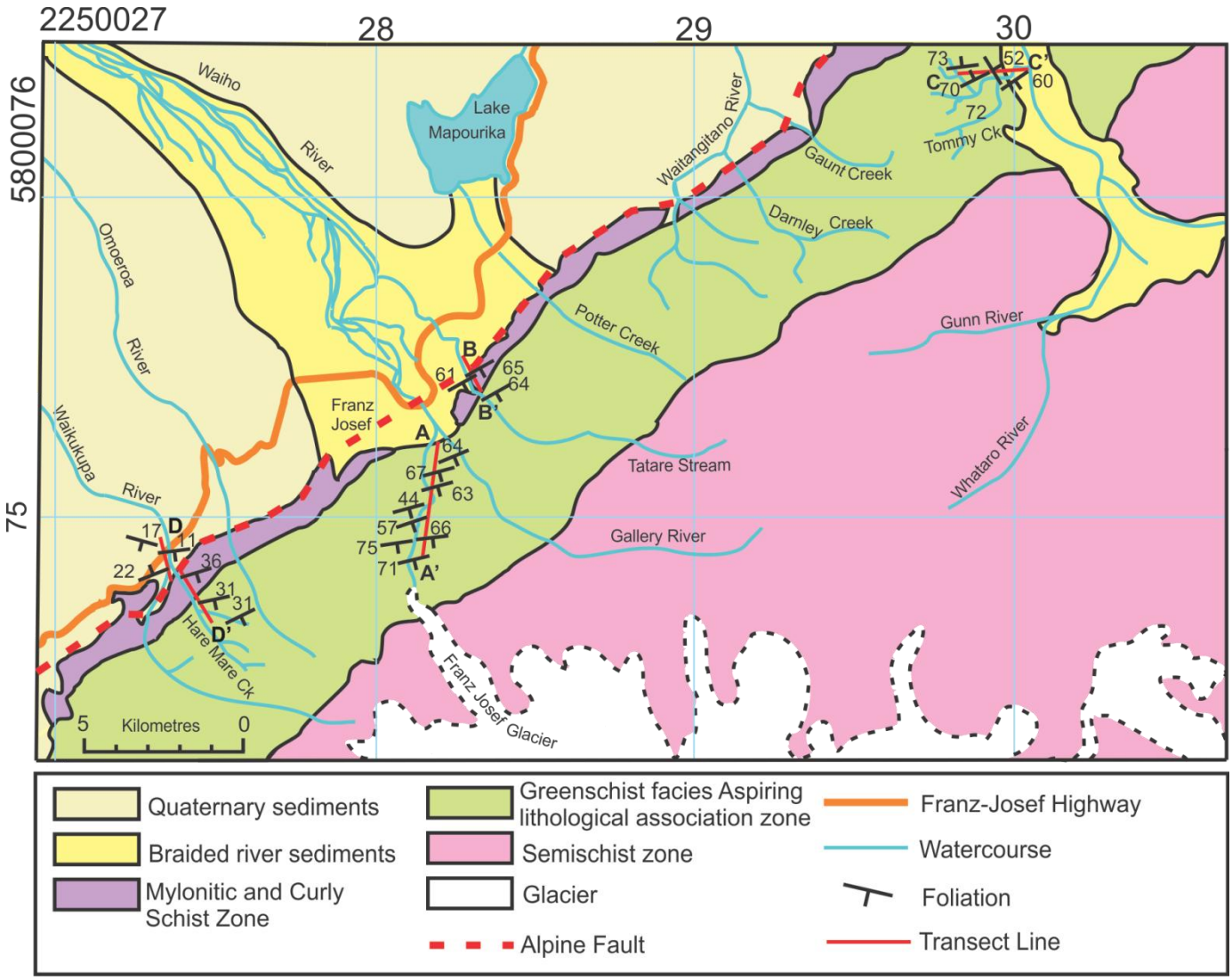


**Figure 2 Geological map of the Central Southern Alps region surrounding the town of Franz Josef, showing variation in geology, general structural trend and schist units with decreasing metamorphic grade east of the Alpine Fault, modified after Cox and Barrell (2007).**

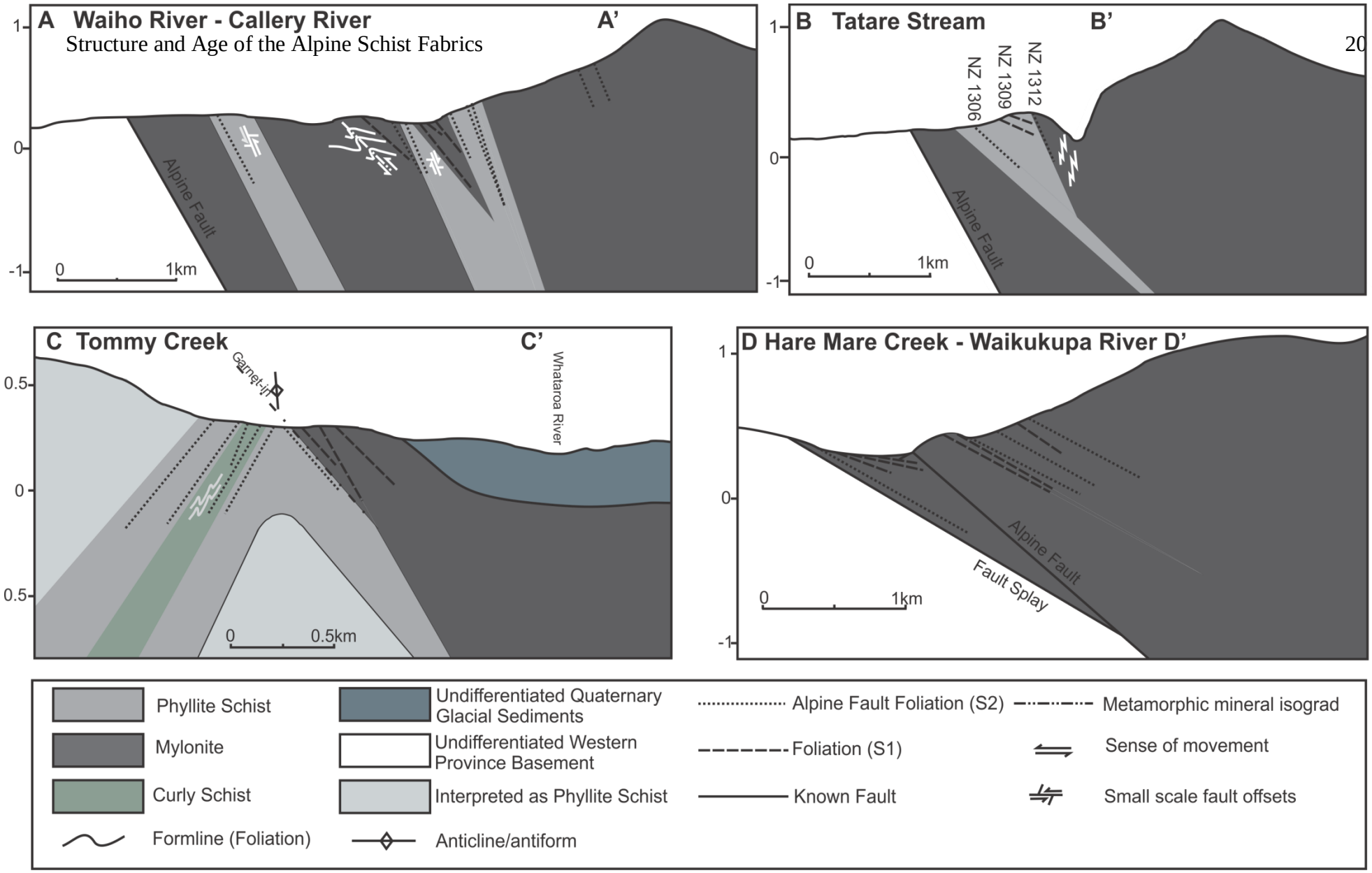


**Figure 3 Geological cross sections (no vertical exaggeration) across the Central Southern Alps region surrounding the town of Franz Josef. See figure 2 for location. A-A' Waiho - Callery River, B-B' Tatare Stream with annotated locations of muscovite samples for $^{40}Ar/^{39}Ar$ dating, C-C' Tommy Creek and D-D' Hare Mare Creek – Waikukupa River. The transect cross sections display schist and mylonite units outcropping at the surface for their length. This is a simplification of the geology of the region to assist with visuallisation as much of the surface is covered by a layer of Quaternary fluvio-glacial sediments that have not been mapped except for the Whataroa river channel. Surface fault expression from the work of Cox and Barrell (2007), fault trace in transect from the seismic interpretation of Davey et al. (1995).**

## TRANSECTS AND STRUCTURAL MEASUREMENTS

The structural measurements recorded from each transect are plotted in Figure 3, the structural measurements and their gps coordinates are available in the appendix, Supplementary Table 2 and 3. The limited and highly weathered outcrop restricted the availability of lineation readings. The foliation measured was defined by the growth of muscovite, plagioclase, biotite and quartz with garnet present as porphyroblasts.

### Waiho River – Callery River Transect

In Figure 4a, the foliation and lineation readings from the Waiho River – Callery River transect are plotted. Within the examined outcrop, no direct cross cutting foliation relationships were observed. From examination of the plotted poles to bedding there are two distinct populations of foliation poles, the dominant steeper foliation plotted in green and the shallower foliation plotted in red. The general trend of the steeper foliation plane plots at 68/130. The general trend of the shallower foliation plane plots at 43/139. No lineation measurements could be taken from the outcrop of the shallower foliation. The lineation poles of the steeper foliation population plot in the south west. Mylonite units are present along the Callery River outcrop, defined by 2-5 cm wide lenses of quartz strung out along the foliation. Anastomising dark mineral bands grew within the foliation planes. The foliation of the outcrops altered between fine 1-0.5 mm and 7 mm foliation, defined by biotite and muscovite-quartz. Minor low angle quartz veins cross cut the foliation. The occurrence of minor centimetre scale propagation folds show thrusting east over west with deformation of the fabric. The west down thrusting relationship is also displayed in the minor small scale fault offsets examined in the outcrop. A minor east down relationship was found in the same outcrop that hosted the larger west down faults.

## Tatare Stream Transect

The Tatare Stream transect measurements are plotted in Figure 4b. Without evidence of direct cross cutting foliations, the same population assignments used to categorise the Waiho River – Callery River transect foliation poles were applied. The steep foliation plane plots at 64/140 and the shallow foliation plane plots at 53/149. The lineation readings all plot in the southwest and do not display a different orientation relationship between the categorised shallower and steeper foliation pole populations. Joint sets spaced ~0.5 metres apart were present, dipping steeply to the west within the Alpine Schist outcrop. At the centimetre scale regions of the foliation would bend into a shallow C' shear with a prominent east down orientation. Within the phyllitic and mylonitic unit, at the centimetre, scale micaceous minerals defined a shortening vector 90 degrees to the foliation with prominent C-S fabrics defined by micaceous mineral growth displaying an east down trend. The phyllite unit contained large quartz veins parallel to the foliation. Minor quartz veins cross cut the mylonitic foliation. Zones of actinolite growth were hosted within the shear with foliation aligned and random anastomising mineral growth that cross cut the foliation. Banding between garnet rich zones with associated actinolite growth and quartz rich bands with no actinolite growth were minor features of the actinolite zones. The zones of random actinolite growth were associated with the finer grained, steeper foliation. Minor west verging asymmetric parasitic z-folds were present within the mylonitic unit.

## Tommy Creek Transect

The foliation readings from the Tommy Creek transect are plotted in Figure 4c. There are 3 distinct populations of foliation readings, the steep south east foliation plotting at 72/131, shallow south east foliation plotting at 51/130 and the north westerly plotting foliation with a general trend of 72/345.

A prominent feature of the Tommy Creek transect is the kilometre scale antiform structure interpreted from the change in foliation measurements. The hinge of the fold plunges 33→062. Within the region of the fold hinge units are highly fractured and milled in parts. Fine grained tight 1-3 cm crenulations are separated from zones of larger crenulation folds of 5-10 cm comprised of coarse quartz veins. The axis plane of the small folds and crenulations strike east northeast. Finer grained minerals are generally associated with steeper foliation. At the western extent of the transect, a metre scale zone of highly fractured rock with numerous small scale shears displayed an east down relationship. This fracture zone was present between thick metre scale zones of unfractured foliation.

### Hare Mare Creek – Waikukupa River Transect

In Figure 4d, the foliation poles and lineation of the Hare Mare Creek – Waikukupa River transect are plotted. The foliations generally are shallower in orientation than the previous transects but can still be categorised into 2 distinct south easterly foliations and a north westerly foliation. The general trend of the two south westerly foliations are 33/132 and 16/139 for the shallow foliation. The north westerly foliation readings indicate a general trend of 21/294. No evidence of folding was observed along the transect.

The western section of the transect up to the Alpine Fault contact was within the Waikukupa River channel. On the east of the fault contact, outcrop dipped shallowly towards the north west before the Alpine Fault was crossed and the transect line entered the Waikukupa River channel. Downstream in the Waikukupa River channel, the general foliation dip trended to the southeast in similar orientation to the Hare Mare foliation.

The rock units from east to west displayed a decrease in grain size to the Alpine Fault, with a general shallowing of dip to the southeast. Figure 4e plots the lineation readings taken from all the transects. The lineations all plot within the southwest with the exception of the

lineation readings taken from the northern limb of the Tommy Creek fold that plot to the west.

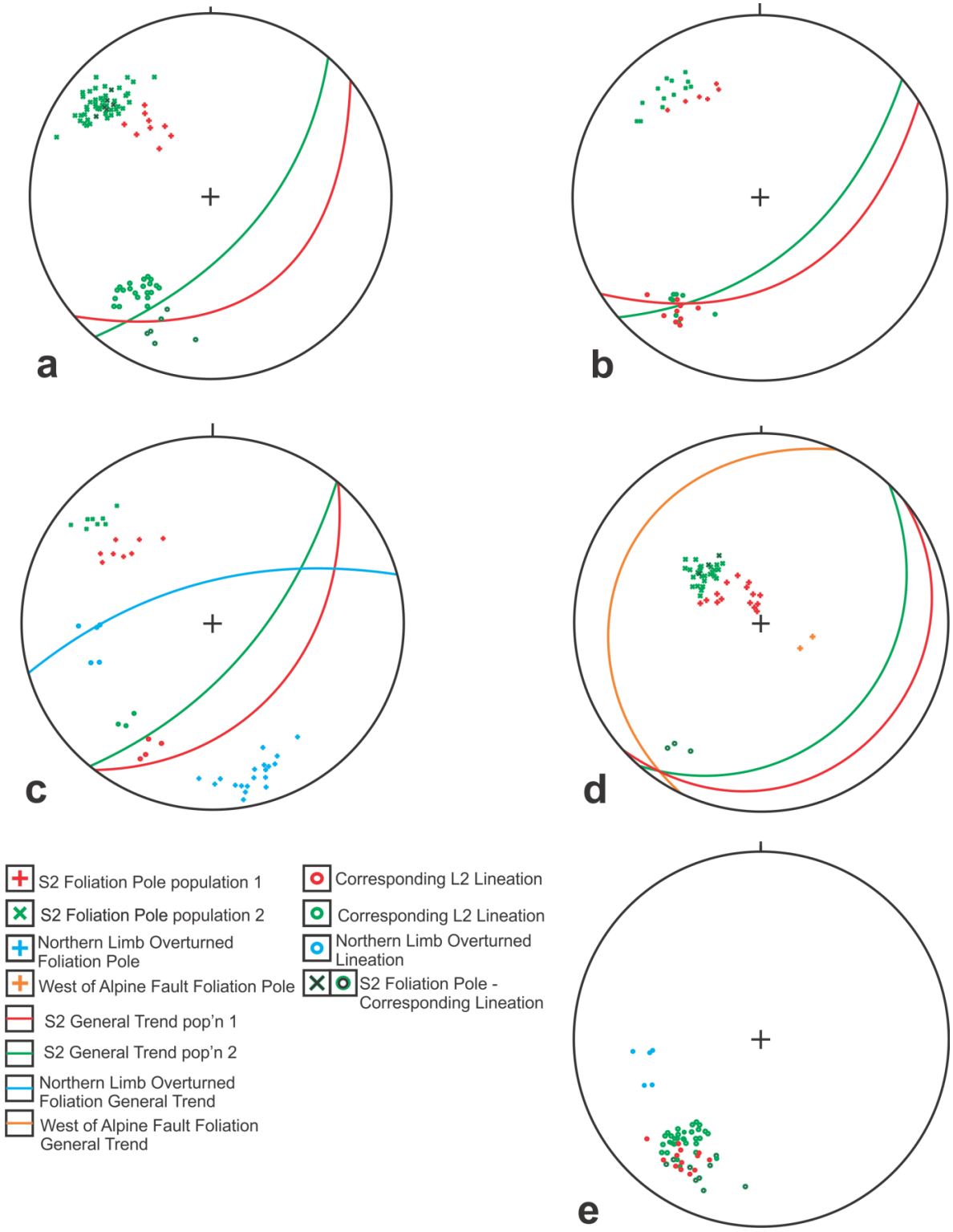


**Figure 4 Foliation and lineation readings collected from transects seen in figure 3. (a) Waiho River – Callery River transect (Poles to foliation, lineation, foliation trend), (b) Tatare Stream transect (Poles to foliation, lineation, foliation trend), (c) Tommy Creek transect (Poles to foliation, lineation, foliation trend, calculated fold axis), (d) Hare Mare Creek – Waikukupa River transect (Poles to foliation, lineation, foliation trend), (e) All lineation readings. Where there are discrete populations of foliation measurements these are identified by different colours on the stereonets.**

## U/Pb Laser Ablation Inductively Coupled Mass Spectrometry Data

Initially 8 thin sections were cut to identify garnet porphyroblasts with in-situ monazite, titanite and zircon with the aim of dating porphyroblasts inclusions to constrain the fabric age. The absence of monazite, titanite and zircon in the thin sections resulted in the need for analysis of separated zircon.

Zircon yields from the Alpine Schist samples were low and dateable grains were found in only 3 samples. The samples and the analysed grains are presented in Table 7.

**Table 7 Zircon grains and concordance data**

| Sample | Total Grains | Laser Spots | 10% Concordance Analysis Spots | 5% Concordance Analysis Spots |
|---|---|---|---|---|
| **NZ1309** | **6** | **14** | **10** | **7** |
| **NZ1310** | **34** | **89** | **47** | **26** |
| **NZ1315** | **5** | **12** | **3** | **3** |

The samples were analysed to characterise the age of the zircon cores and any change in age within the rims of the grains. The full dataset carrying the results of all laser analysis is included in the appendix, Supplementary Table 1.

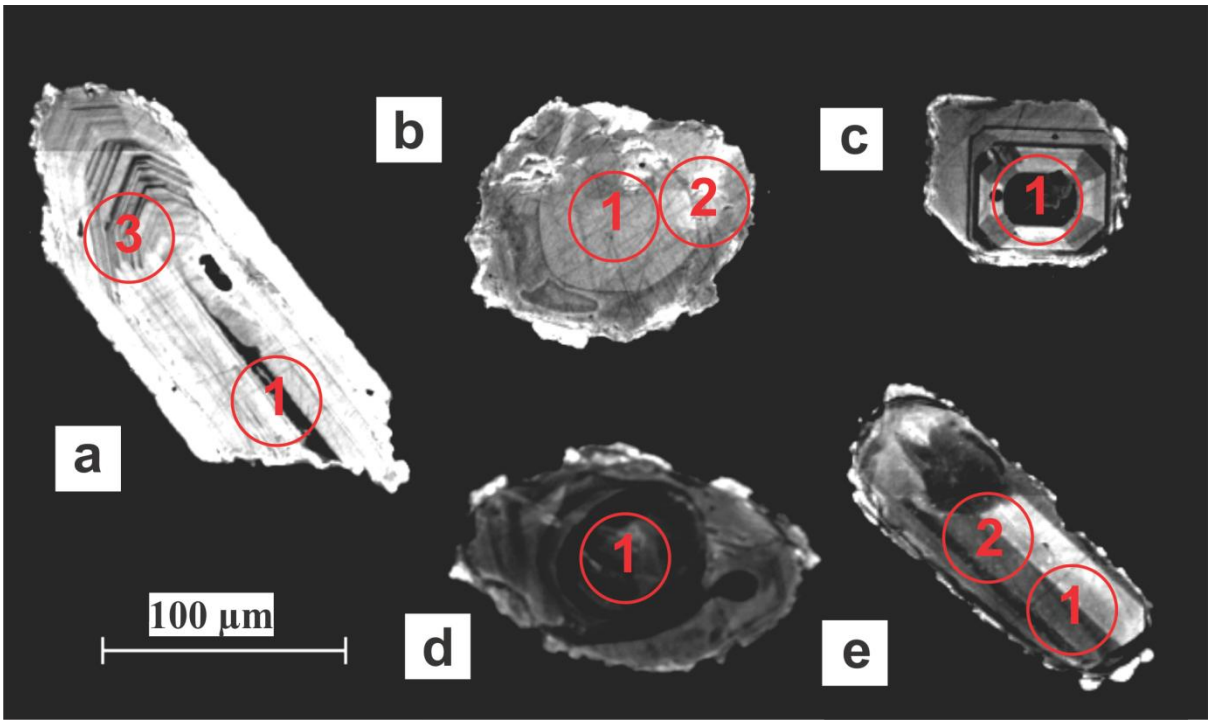


**Figure 5 CL imaging of zircons separated from Alpine Schist samples with laser spots annotated in red. (a) Sample NZ1310_Z5, growth zoning in typical crustal rocks, dark and bright zoning (a1 126.6 ± 1.8 Ma, a3 124.8 ± 1.8 Ma), (b) Sample NZ1310_Z15, homogenous xenocrystic core with polishing scratches, inner rim, evidence of metamorphic inner rim and bright outer rim, (b) 139.1 ± 3.3 Ma, b2 124.8 ± 3.3 Ma), (c) NZ1309_Z1 Growth zoning typical of crustal rocks, minor bright outer rim, (c1 265.9 ± 3.5 Ma), (d) NZ1310_Z25 metamorphic core with non homogenous outer rims, (683.1 ± 8.8 Ma), (e) NZ1210_Z24 well defined zones of core, bright and dark, with bright outer rim sections (e1 3345.4± 33.9 Ma, e2 3251.3 ± 33.9). Locations of concordant laser spots numbered for each zircon. All ages $^{238}U/^{206}Pb$ ages.**

## Zircon textures

Typical zircon texture CL images from the Alpine Schist sample are presented in Figure 5. Zircons are characterised by their textures following the method of Corfu et al. (2003).

A total of 6 zircon grains were separated from sample NZ1309. The zircons are all ~ 100 µm in length, sub angular to prismatic. The CL imaging in Figure 5, demonstrates that most zircon consists of a relict core displaying characteristic magmatic oscillatory growth zoning with irregular overgrowth rims. Many of the zircons were fractured but did not display overgrowth along fractures. A common feature of the zircon grains was the presence of a partially formed bright rim as seen in Figure 5d and 5e. A typical magmatic textured core from the sample is presented in Figure 5c.

Within sample NZ1310, a total of 34 zircons were separated. Zircons ranged from ~50-200 µm with sub-angular, sub-rounded and prismatic grains. Within the grains core minor pits/inclusions were present as dark spots in the CL image, as seen in the core of the zircon in Figure 5a. The prismatic and oscillatory zoned magmatic grains were the most abundant zircon. Many of the elongate grains were fractured and showed evidence of rim formation along the fracture edge with bright blobs along the grains edge. The typical magmatic core and magmatic rim showing irregular zoning is seen in Figure 5b. Typical metamorphic core and irregular metamorphic zoning is displayed in Figure 5d.

Only 5 grains were separated from the hand sample of NZ1315. The zircons are ~50-100 m. Of these 2 displayed magmatic cores and oscillatory zoning. Within the metamorphic core zircons, complex overgrowth patterns were formed with a series of cross cutting and irregular zones. The outer rim was characterised by a bright zone of alteration affecting the zircons and crystallising along fractures within the zircon pits.

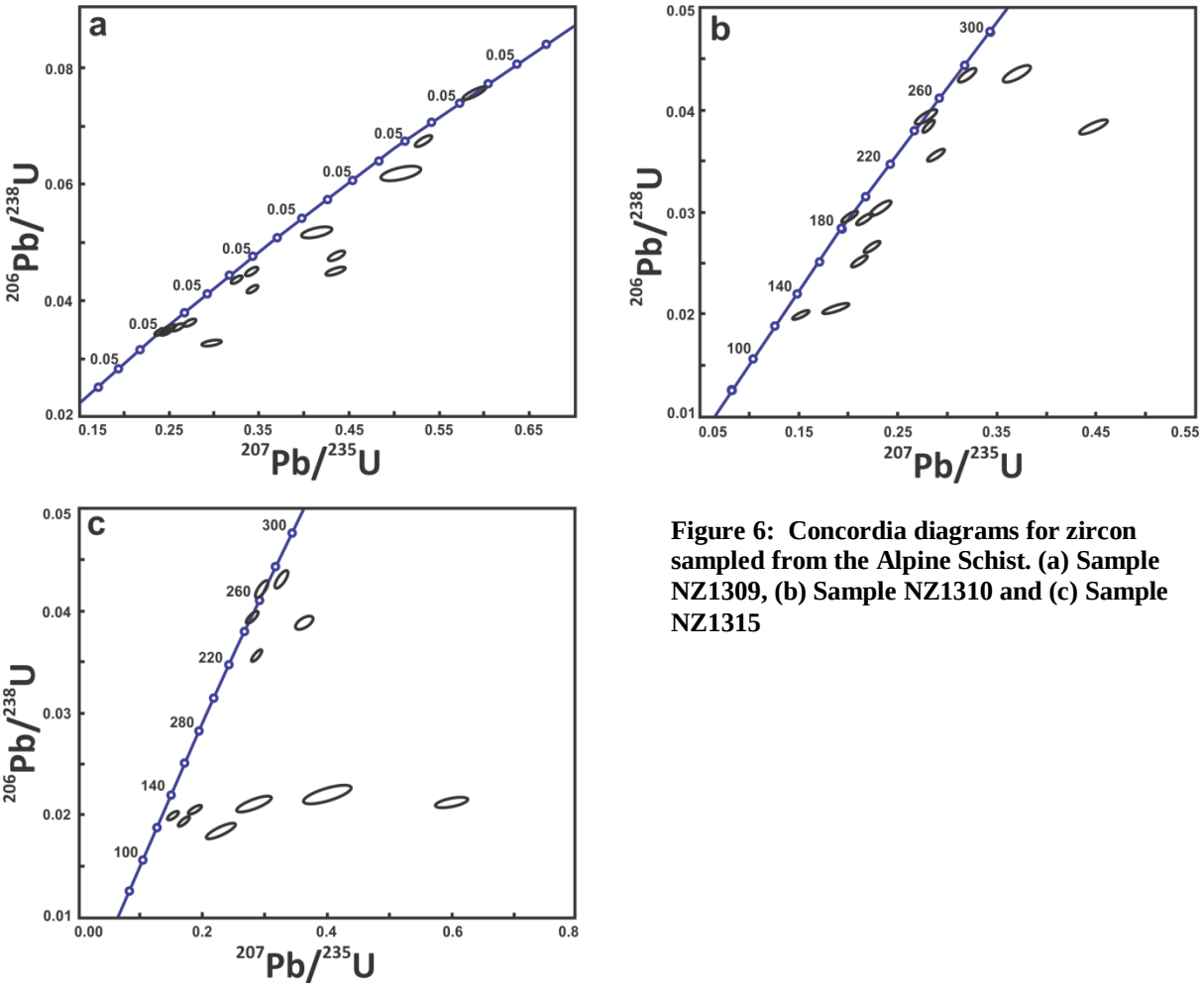


**Figure 6: Concordia diagrams for zircon sampled from the Alpine Schist. (a) Sample NZ1309, (b) Sample NZ1310 and (c) Sample NZ1315**

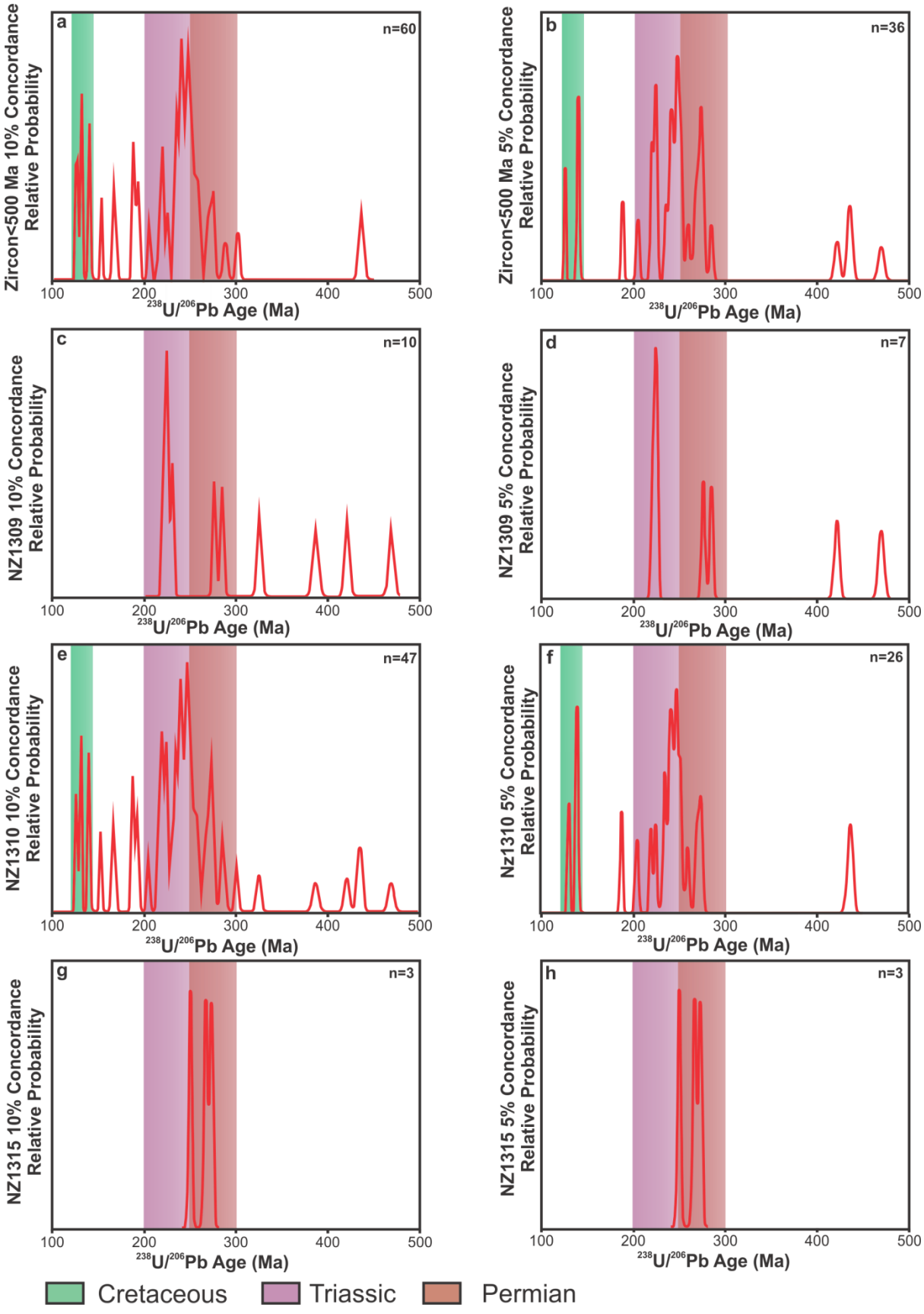


**Figure 8 $^{238}U/^{206}Pb$ detrital zircon age <500 Ma, relative probability plots for (a-b) Alpine Schist (NZ1309, NZ1310, NZ1315), (c-d) NZ1309, (e-f) NZ1310, (g-h) NZ1315. Data at discordance <10% (a, c, e, g) and <5% (b, d, f, h) are used here for comparison. Prominent peak ages for the Cretaceous occur at ~124 Ma and ~140 Ma. The Triassic peak ages occur at ~220 Ma and ~240 Ma. Permian peak ages occur at 260 Ma and 270 Ma. Minor Silurian ages occur around 430 Ma. A singular Ordovician peak occurred at ~470 Ma. All ages $^{238}U/^{206}Pb$ Age.**

## Data of Alpine Schist samples

The age data for the three samples with ages younger than 500 Ma are presented in relative probability plots at the 10% and 5% concordance level in Figure 5.

Sample NZ1309

Prominent peak ages at 5% concordance seen in Figure 6d occur in the Triassic at ~220 Ma with minor analyses peaks in the Permian, Silurian and Ordovician. The Triassic and Permian age zircons are characterised by metamorphic cores and bright irregular metamorphic rims. The zircons of Silurian and Ordovician age have magmatic cores.

Sample NZ1310

Prominent age peaks occur in the Cretaceous with the youngest age at 124.6 ±1.8 Ma (1σ) and in the Triassic around ~220 Ma and major peak around ~240 Ma with minor peaks present in the Jurassic at ~180 Ma and Ordovician at ~470 Ma as seen in Figure 5f. The Cretaceous aged grains are associated with magmatic cores. The Triassic peaks at ~240-230 Ma were cores with younger ~200 Ma rims. The Permian peak was associated with both metamorphic and magmatic zircon cores.

Sample NZ1315

The zircon extracted comprised 2 zircon. The youngest a metamorphic zircon, seen in Figure 5h, with a Triassic age of ~249 Ma and 1 zircon with Permian ages of ~272 Ma and ~265 Ma in the core and rim respectively.

The Ordovician zircons presented magmatic grains. The Silurian grains also presented magmatic zircons. With the Permian aged zircons there were magmatic and metamorphic cores and rims. The Triassic grains were characterised by magmatic zircon. The Jurassic zircons were characterised by metamorphic grains. The Cretaceous grains showed magmatic cores overgrown by metamorphic rims. Indicating the youngest detrital grains are of Triassic age.

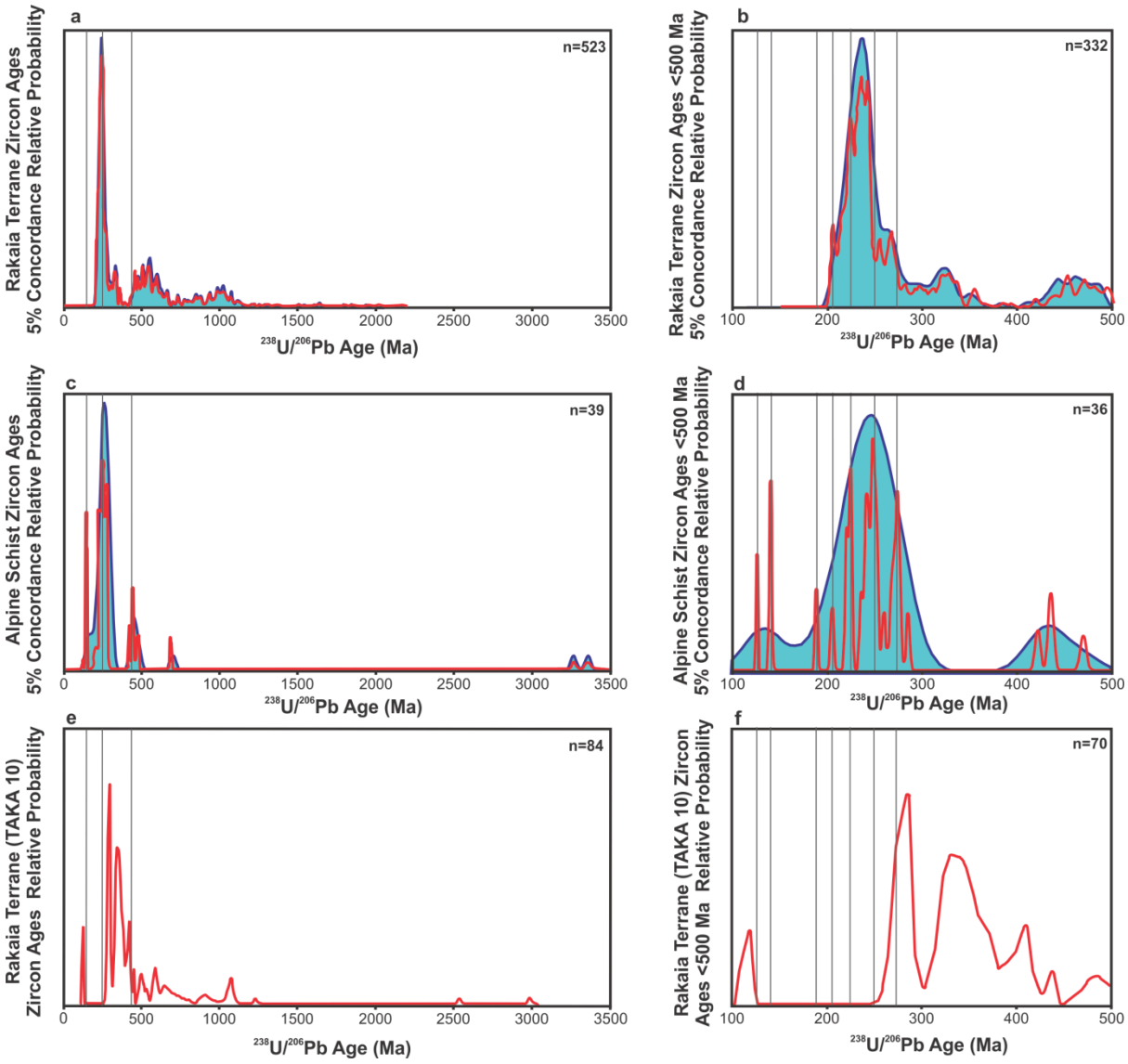


**Figure 9 $^{238U}/^{206}$Pb detrital zircon age relative probability plots with kernel density plots following the method of Vermeesch (2012) for, (a-b) Rakaia subterrane (Torlesse terrane) from unpublished ages of (Acott 2013), (c-d) Alpine Schist (NZ1309, NZ1310, NZ1315) and (e-f) U/Pb detrital zircon age relative probability plots of Rakaia subterrane (Torlesse terrane-Haast Schist Transition Zone) sandstones (TAKA10) from Pickard et al. (2000). Relative probability plots show all data within discordance <5%. Prominent populations are correlated between plots with grey vertical lines.**

## AGE COMPARISON OF ALPINE SCHIST AND RAKAIA TERRANE ZIRCON

### Rakaia Terrane Samples of Acott (2013)

The Rakaia Terrane oldest ages plotted in Figure 9a are minor Proterozoic age analyses. The samples <500 Ma plotted in Figure 9b correspond with a prominent Palaeozoic relative probability peak and kernel in the Triassic.

### Alpine Schist Zircon

All Alpine Schist zircon analyses are plotted in Figure 9c, with analyses <500 Ma plotted in Figure 9d. The oldest Alpine Schist zircon analysis is Archaean with a single analysis peak in the Proterozoic. The analysis younger <500 Ma plot a prominent Paleozoic kernel corresponding to Silurian and Ordovician relative probability analysis peaks. The prominent kernel population ~200-300 Ma corresponds to analysis peaks in the Permian and Triassic with a minor Jurassic component. The kernel peak is older than that of the Rakaia Terrane main kernel peak in Figure 9b. The Alpine Schist Cretaceous kernel corresponds to the youngest analysis at ~124 Ma.

### Rakaia Terrane (TAKA10) Samples of Pickard et al. (2000)

All TAKA10 analyses of Pickard et al. (2000) are plotted in Figures 9e with ages <500 Ma plotted in Figure 9f. The oldest TAKA10 zircons plot in the Archaean at younger ages than the Archaean age peak in the Alpine Schist. The TAKA10 samples show a Proterozoic distribution of ages in Figure 9e. The TAKA10 ages <500 Ma, in Figure 9f, plot analysis peaks in the Silurian, Carboniferous and Permian. The youngest TAKA10 samples analyses are Cretaceous at ~110 Ma.

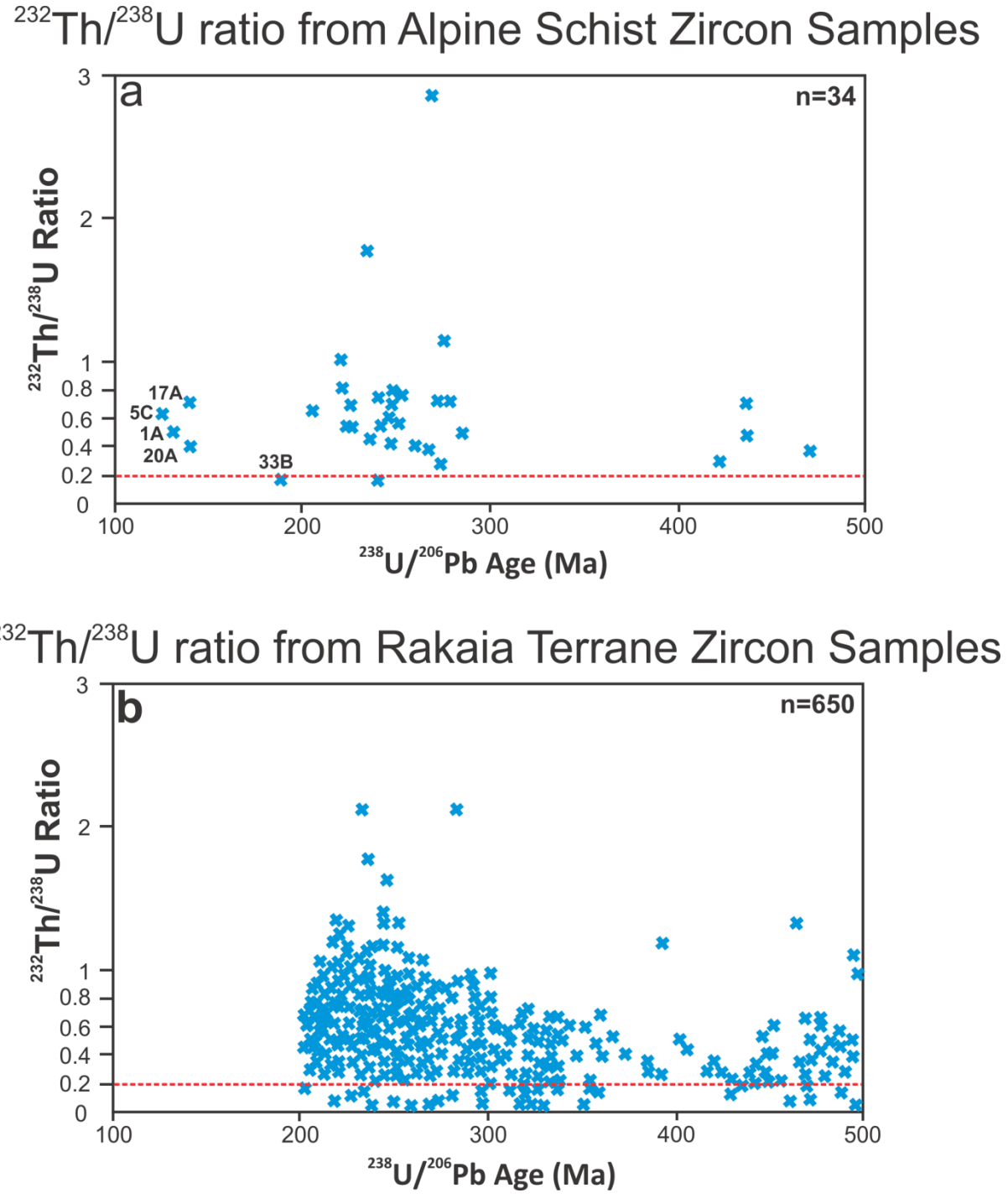


**Figure 10 (a) $^{232}Th/^{238}U$ Ratio from Alpine Schist zircon samples plotted against $^{235}U/^{206}Pb$ Age for samples <500 Ma with annotated samples 10_5C at 124.6 Ma $^{232}Th/^{238}U$ 0.63, 10_1A at 130.2 Ma $^{232}Th/^{238}U$ 0.51, 10_20A at 139 Ma $^{232}Th/^{238}U$ 0.415, 10_17A at 139.1 Ma $^{232}Th/^{238}U$ 0.713. and NZ1310_33B at 187.5 ± 2.6 Ma ) $^{232}Th/^{238}U$ 0.17(b) Th/U Ratio from Rakaia Terrane Zircon Samples plotted against their $^{235}U/^{206}Pb$ Age for samples <500 Ma.**

## $^{232}Th/^{238}U$ ratio comparison of Alpine Schist and Rakaia Terrane zircon

The dashed line in Figure 10 provides a generalised signature of metamorphic and magmatic zircon origin, following the classification of Timms et al. (2006), the following signatures are indicated, $^{232}Th/^{238}U$ <0.2 Metamorphic and $^{232}Th/^{238}U$ magmatic origin.

The $^{232}Th/^{238}U$ ratios from the Alpine Schist zircon show values greater than 0.2 at all ages, except for the 2 samples listed in Table 8.

**Table 8 Table of Alpine Schist Zircon samples with an Th/U ratio<0.20**

| Sample | $^{232}Th/^{238}U$ Ratio | Age (Ma) |
|---|---|---|
| 2_10_33B (rim) | 0.172159833 | 187.5 |
| 2_10_10C (rim) | 0.177070399 | 239.5 |

From the Rakia Terrane as seen in Figure 10 b, a total of 34 zircons had $^{232}Th/^{238}U$ ratio less than 0.2 with 8 of these occurring in the Triassic, 7 within the Permian and 3 within the Ordovician.

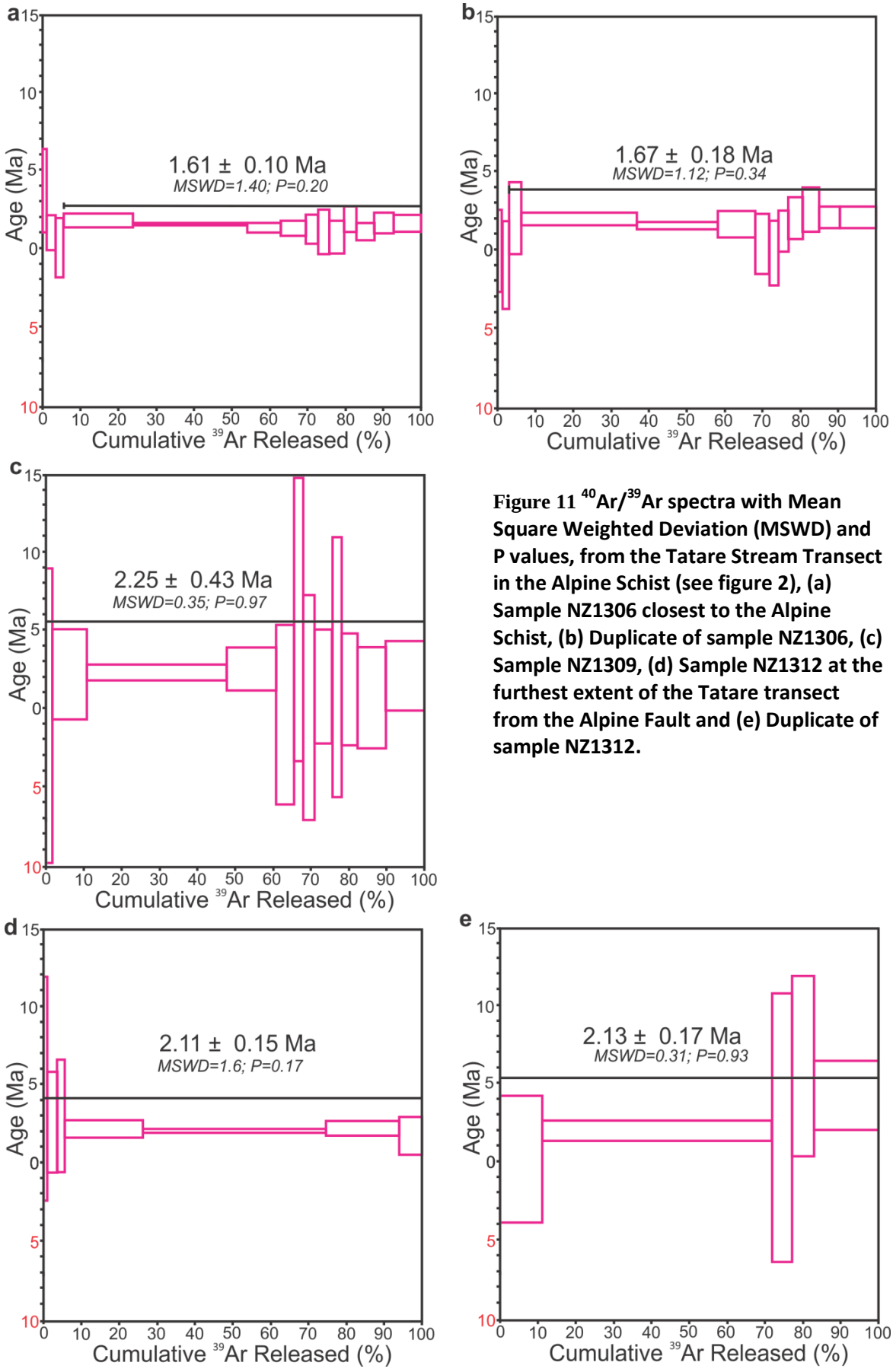


**Figure 11 $^{40}$Ar/$^{39}$Ar spectra with Mean Square Weighted Deviation (MSWD) and P values, from the Tatare Stream Transect in the Alpine Schist (see figure 2), (a) Sample NZ1306 closest to the Alpine Schist, (b) Duplicate of sample NZ1306, (c) Sample NZ1309, (d) Sample NZ1312 at the furthest extent of the Tatare transect from the Alpine Fault and (e) Duplicate of sample NZ1312.**

## ALPINE SCHIST MUSCOVITE $^{40}AR/^{39}AR$ ANALYSES

It can be seen in the Figure 11, that all the muscovite $^{40}Ar/^{39}Ar$ age analysis exhibit a Pleistocene distribution. Comparing the age data present in Table 9, with the annotated transect in Figure 3 the youngest age (1.62 ± 0.09 Ma) is present closest to the Alpine Fault. In relation to the cross section of Tatare Stream in Figure 3, the age distribution shows a general decrease in age towards the Alpine Fault, with the exception of the shallow foliation data at the location of sample NZ1309, at this location age increases out of trend. Taking into account the errors of the samples with the overlap between samples NZ1309 and NZ1312, the data shows a general trend of decreasing $^{40}Ar/^{39}Ar$ age on approach to the fault.

**Table 9 $^{40}Ar/^{39}Ar$ age of samples presented with reference to elevation and surface distance from the Alpine Fault, interpreted using gps coordinates in Table 3 and fault trace mapped by Cox and Barrell (2007)**

| Sample | NZ1306 (Combined) | NZ1309 | NZ1312 (Combined) |
|---|---|---|---|
| Age (Ma) | 1.62 ± 0.09 | 2.25 ± 0.43 | 2.10 ± 0.15 |
| Elevation (m) | 200 | 220 | 240 |
| Distance from Alpine Fault trace (m) | 1090 | 1230 | 1570 |
| MSWD | 1.20 | 0.35 | 0.83 |
| P value | 0.24 | 0.97 | 0.66 |

## Discussion

The present study has focussed on various aspects of the foliation structure and geochronology of the minerals zircon and muscovite from within the Alpine Schist. The structural measurements have been used to orient the foliation in relation to the active Alpine Fault. Zircon geochronology was performed to investigate the provenance of the sediments within the Alpine Schist and compare this with the Rakaia Terrane of the Torlesse Supergroup. Zonation of the zircon minerals was examined to identify overgrowth of the grains and subsequent geochronological analyses were used to determine the growth history of the zircons and develop an understanding of the progression of zircon crystallisation as an indicator of high grade metamorphism within the rocks of the Alpine Schist. Muscovite is a dominant fabric forming mineral within the rock units of the Alpine Schist. The muscovite $^{40}Ar/^{39}Ar$ geochronology allowed for the investigation of the age of this dominant fabric mineral and age relationship with the formation of the Alpine Schist fabric.

## Structural Data

Partitioning of Strain – Cenozoic Fabrics

The fabrics observed within the transects give an indication of the strain environment that is created by uplift along the Alpine Fault (Toy et al. 2008). There are two fabrics a dominant steeper foliation that approximates the dip of the Alpine Fault and a minor shallow foliation population. As the fault is approached orientation in line with the fault is dominant indicating that the exhumation rate and strain is greatest at the fault (Toy et al. 2008).

The shallower foliation poles may reflect decreased rates of exhumation and strain away from the fault, folding or may be attributed to observed thrust-duplexing, thrust segmentation and gravity collapse structures observed in the Alpine Schist (Sibson et al. 1981, Norris and Cooper 1995, Norris and Cooper 1997). The orientation of small scale shears and faults in

line with the orientation of the Alpine Fault indicates that the current strain is aligned with the fault, suggesting a continuation of Pliocene strain. The cross cutting C' fabrics within the phyllite are indicators of an active surface tracking toward the principle plane of finite strain.

Small scale evidence of heterogenous strain partitioning

Within the outcrop numerous small scale features exhibited heterogeneous shearing providing evidence of strain partitioning during uplift of the Alpine Schist (Toy et al. 2008). The occurrence of east down and west down shear relationships deforming the Alpine Fabric with sense of movement orthogonal to the Alpine fault indicates variable strain partitioning between the Alpine Schist rock units. The general trend of decreasing grain size on approach to the fault indicates increasing strain linked to increased uplift at the fault (Toy et al. 2010, Toy et al. 2008).

Evolving Stress Field

Within the Tatare Stream and Waiho River transects the growth of actinolite, both oriented with the foliation and anastomising growth, cross cutting the foliation within adjacent foliation layers, indicates that this mineral had growth within the fabric forming strain field and retrograde mineralisation at temperatures between 500-550$^{o}$ C (Little et al. 2005). The presence of the random actinolite growth away from the fault suggests a decreasing strain component away from the fault. Dating the ages of the alternate growths would in part constrain the age relationship of the strain environment; unfortunately there was not time within this project to generate hornblende $^{40}Ar/^{39}Ar$ age data.

## Zircon Analyses

### ALPINE SCHIST MAXIMUM DEPOSITIONAL AGE

The maximum depositional age for the individual samples is here interpreted to be defined by the youngest <5% discordant $^{238}U/^{206}Pb$ analysis of detrital zircon. The maximum depositional age of the three samples NZ1309, NZ1310 and NZ1315 analysed here are 219.8 ± 3.4 Ma, 204.1 ± 3.5 and 248.9 ± 3.7 respectively. These ages indicate that the protoliths for the Alpine Schists were deposited in, or after, the Triassic.

### AGE PROVENANCE OF THE ALPINE SCHIST ZIRCON

In this section I aim to discuss the detrital zircon ages from the three samples from which data was collected. The data are discussed together because the samples are from similar structural positions in rocks that have previously been correlated in the same tectonic unit (Little et al. 2002).

Within the Alpine Schist detrital zircon analyses, age maxima, occur in the Archaean, Proterozoic, Ordovician, Silurian, Permian and Triassic. The peaks within the Jurassic and Cretaceous are younger than the interpreted maximum depositional age for the Alpine Schist as they are interpreted to have formed in situ. The detrital zircon with Archaean cores at ~3.3 Ga with a ~3.2 Ga rim, is likely to be sourced from the Australian continental crust (Pickard et al. 2000). However, zircon of this age could come from many sources with sediment cycling through earlier orogens and the provenance of many Pre-Cambiran zircon unkown (Adams et al. 2007). It is proposed by Gibson and Ireland (1996) that detrital zircon of this age is incorporated from an eroded fragment of Archaean basement of the Delamerian Orogen that rifted from Gondwana ~480 Ma. The Ordovician to Silurian detrital zircon components have possible source regions within the Hodgkinson Province of Northern

Australia (Adams et al. 2007). It is proposed by Vos et al. (2006) that an arc magmatic source provided Ordovician aged zircon to the Hodgkinson Province of northern Queensland. An alternative source of Ordovician zircon comes from magmatism in the Macquarie Arc of the Lachlan Fold Belt (Percival and Glen 2007). Deposition of sediment from the southern Macquarie Arc source could have occurred after southern migration of the Alpine Schist depocentre, that occurred during the Permian-Triassic (Pickard et al. 2000).

The Georgetown Inlier is a host of Silurian granitic plutons that are a likely source of Silurian zircon within the sample (Withnall et al. 1997). The major Late-Middle Permian detrital zircon analyses in the sample is proposed to have originated in the New England Orogen, with exhumation and erosion linked to the Hunter-Bowen event (~270-280 Ma), leading to deposition in the Alpine Schist depocentre (Adams et al. 2007, Pickard et al. 2000). The Triassic grains are likely sourced from southern areas of Queensland due to migration of the depocentre south in the Permian-Triassic. This region was host to voluminous granitoids relating to the New England super suite that were emplaced between ~230-250 Ma (Pickard et al. 2000).

The Jurassic aged zircon (~187 Ma) is interpreted to have formed in situ and may have formed during the onset of the Rangitata Orogeny ~190 Ma (Grapes 1995) in time with the onset of high grade metamorphism in the Otago Schist (Mortimer and Cooper 2004). An alternative possibility is that the single Jurassic zircon is detrital although its analysed $^{232}Th/^{238}U$ ratio suggests a metamorphic origin. There are minor Jurassic detrital zircons within the Pahau Terrane, neighbouring the Rakaia Terrane to the east (Adams et al. 2007). Within the Pahau Terrane, Jurassic arc magmatic sources, on the eastern margin of New Zealand, are a more likely source than Australian continental sources with possible formation in the Median Batholith (Wandres et al. 2004, Adams et al. 2007).

The youngest zircon ages across all samples were found in the Cretaceous. The zircon analysis ~139-124 Ma are older than the extension related metamorphism deformation of 100-110 Ma that exhumed higher grade units across New Zealand (Mortimer and Cooper 2004). These ~139-124 Ma ages are likely to be related to the Late Cretaceous formation of higher grade units within the Alpine Schist relating to crustal thickening that occurred before the Cretaceous opening of the Tasman Sea (Vry et al. 2004).

This discussion on the age provenance of detrital zircon within the Alpine Schist is limited in nature due to the small sample of detrital zircon that could be separated from the rock. To provide greater strength to the discussion further zircon samples should be collected to develop a greater understanding of the detrital zircon age distribution.

## COMPARISON OF ZIRCON AGE ACROSS ALPINE SCHIST AND RAKAIA TERRANE

The distribution of zircon ages from the unpublished Rakaia Terrane data of Acott (2013) and TAKA10 Rakaia Terrane data of Pickard et al. (2000) was compared with the ages of the Alpine Schist samples to examine provenance of the three samples. Examination of this assists in determining the likelihood of the Rakaia Terrane being the protolith of the Alpine Schist. The comparison relative probability plots in Figure 7 exhibit homogeneity between the protolith depocentre sediments of the samples. Within Figure 7a, c and e the Proterozoic and Archaean zircon analysis are variable and low between the three samples. The plots of analyses younger than 500 Ma, exhibit common relative probability analysis peaks and kernels. All samples contain Ordovician –Silurian zircon populations. The Rakaia Terrane data of Acott (2013) and TAKA10 data of Pickard et al. (2000) contain Carboniferous zircon. The TAKA10 sample and Alpine Schist sample have prominent Permian peaks absent in the Rakaia terrane sample, however the TAKA10 sample peak is earlier in the Permian than the Alpine Schist Permian populations. Within the Triassic the Rakaia Terrane and Alpine schist

have corresponding kernels while the TAKA10 sample shows no analyses of this age. The Alpine Schist is the only sample with Jurassic analysis, consisting of a single zircon. The youngest analyses are Cretaceous in the TAKA10 and Alpine Schist samples. The TAKA10 sample has the youngest Cretaceous age at ~110 Ma compared to the ~124 Ma age of the Alpine Schist zircon analyses.

## SEDIMENT PROVENANCE OF RAKAIA TERRANE AND ALPINE SCHIST

The common Silurian and Ordovician ages corresponding to the Palaeozoic kernels in the Alpine Schist and Rakaia Terrane samples are consistent with a common provenance of sediment from the Hodgkinson Hinterland (Adams et al. 2007).

The absence of Carboniferous zircon within the Alpine Schist samples may result from variable sediment supply during this time period to the Alpine Schist depocentre or may only reflect the smaller sample size of the Alpine Schist. Within the Rakaia depocentre it is proposed by Wandres et al. (2004) that the Carboniferous granite complexes of New South Wales are a probable source of these zircon in the Rakaia Terrane.

The Permian age gap of the Rakaia samples of Acott (2013) correlates to the absence of Australian igneous activity of this age (Wandres et al. 2004). The Permian zircon within TAKA10 and the Alpine Schist regions is proposed by Wandres et al. (2004) to have originated from the Kohler Range granitoid. The less voluminous Kohler Range compared to the large New England Fold Belt source may explain the lower Permian sediment source in the Rakaia samples with deposition favouring the easterly Alpine Schist and TAKA10 depocentres.

There is little evidence of magmatic arcs along the east of New Zealand in the Permian restricting source regions to the Australian continent (Adams et al. 2007)

The prominent Triassic component across the Rakaia and Alpine Schist samples correlates to the voluminous New England Fold Belt as a proximal source of sediment (Adams et al. 2007) combined with the eastward migration of the TAKA10 from the Australian continental margin, starving it of Triassic Sediment with no evidence of coastal arc magmatic activity at this age providing a proximal sediment source (Pickard et al. 2000).

After Triassic deposition the Rakaia terrane samples of Acott (2013), records no younger analyses. The absence of Jurassic sediment within the Rakaia terrane relates to the Jurassic rifting or arc magmatic material deposition affecting the westernmost region of New Zealand where the Alpine Schist was deposited leaving the Rakaia unaffected (Grapes 1995, Pickard et al. 2000). The youngest ages of the samples are Cretaceous ages, with the ~110 Ma age of TAKA10 preserving in situ metamorphism (Pickard et al. 2000). The ~124 Ma ages of the Alpine Schist samples do not record the youngest Cretaceous ages of the Alpine Schist, amphibolite garnet samples of Mortimer and Cooper (2004) recording 100 ± 12 Ma ages suggesting high grade metamorphism related to exhumation of the Otago and Alpine Schists. In order to further constrain the provenance of these zircons, Hafnium isotope analysis would be useful for investigating common source regions of sampled zircon. With the available data it is inferred that the Rakaia Terrane is the protolith of the Alpine Schist.

### $^{232}Th/^{238}U$ Ratio of Alpine Schist Zircon

The $^{232}Th/^{238}U$ ratio of zircons from the Alpine Schist and Rakaia Terrane zircon show a majority of values greater than 0.2, suggesting that they formed from a magmatic environment (Timms et al. 2006). The Permian- Triassic ages of this magmatic crystallisation are also the interpreted depositional ages for the Rakaia Terrane and Alpine Schist (Vry et al. 2008).

The Alpine Schist records a suite of zircon age analyses younger than the Rakaia terrane. Of particular note within Figure 10a is the zircon NZ1033 with the laser spot taken from its rim providing a $^{232}Th/^{238}U$ ratio <0.2 at 0.17 with a $U^{238}/Pb^{206}$ age of 187.5 ± 2.6 Ma, the angular nature of the grain suggest in situ growth. This corresponds to the onset of metamorphism from the Rangitata Orogeny ~190 Ma (Grapes 1995).

The Cretaceous population of Alpine Schist $^{232}Th/^{238}U$ signatured magmatic zircons in Figure 10, from ages ~139-124 Ma are of note as there is no known source of magmatic zircon at this age within the Alpine Schist depositional protolith, the nearest Cretaceous ages are the emplacement of subduction arc related magma of the Western Fiordland orthogneiss to the southwest of the Alpine Schist (Mattinson et al. 1986).Deposition of these sediments into the Alpine Schist is unlikely as dominant dextral movement along the Alpine Fault would have isolated these units as a source of sediment before deposition could have occurred.

The core and textures of sample NZ1310_5c display a magmatic $^{232}Th/^{238}U$ signature however the other three samples (NZ1310_20a, NZ1310_17a and NZ1310_1a) show distinct metamorphic textures. The grains do not show evidence of transport suggesting that they formed in situ.

Disagreement between the apparent textures and $^{232}Th/^{238}U$ ratio may just represent natural data variation. Alternatively, disagreement between $^{232}Th/^{238}U$ ratio and zircon textures may result from zircon in the Alpine Schist units adjacent to the Alpine Fault, where peak temperatures reached 480-620 ± 50 $^{o}$C at a pressure of 8-11 Kbars (Cooper 1980, Grapes 1995, Vry et al. 2004), undergoing zircon crystal-plastic deformation. Zircon crystal plastic deformation is documented to have occurred at amphibolites facies by Timms et al. (2006). These unresolved zircons are all less than 100 µm in diameter and their small size may have allowed for crystal plastic deformation to readily occur. Furthermore zircons NZ1310_5c and NZ1310_20a are fractured and have lost fragments providing pathways for crystal-plastic

deformation (Timms et al. 2006) that may have altered the $^{232}Th/^{238}U$ ratios. This may indicate why previous zircon and fabric dating has been diachronous (Vry et al. 2004). From the analysis of $^{232}Th/^{238}U$ ratio and Zircon ages within the Alpine Schist, those ages younger than the Triassic represent metamorphic events.

### $^{40}Ar/^{39}Ar$ Dating of Muscovite

These samples are the first $^{40}Ar/^{39}Ar$ dates to be taken from Alpine Schist near Franz Josef Glacier. Previous K/Ar whole rock ages have been obtained from the region and analysed <2 Ma (Little et al. 2005).These ages assumed that the whole rock had undergone cooling through the same closure temperature and had not undergone later partial reheating/recrystallisation events that may have altered the Argon content (Little et al. 1999). Within the Alpine Schist samples, variation in age vertically and horizontally away from the Alpine Fault seen in Table 9 contrasts with the ages observed within the muscovites south of Fox Glacier that display strong correlation between K/Ar age and elevation (Little et al. 2005). The trend in age distribution decreases toward the Alpine Fault, indicating a thermal or uplift control on $^{40}Ar/^{39}Ar$ age related to fault proximity.

Using the $400^{o}$ C muscovite argon closure temperature of Little et al. (2005), Southern Alp temperature profile of Shi et al. (1996) and the $^{40}Ar/^{39}Ar$ ages calculated in Table 9, within the last ~1.6-2 Ma years, the exhumed rocks were at depths of ~17 km. Within the outcrop samples there is evidence of higher temperature grades with the actinolite in samples NZ1309 and NZ1312 indicating temperatures of ~500-$600^{o}$ C at depth >40 km (Little et al. 2005, Shi et al. 1996), while the garnet of NZ1306 indicate that sample NZ1306 may have been exposed to temperatures ~$600^{o}$ C at ~7-10 kbar (Vry et al. 2004).

These high grade minerals may indicate that the muscovite $^{40}Ar/^{39}Ar$ ages reflect cooling of the samples below $400^{o}$ C and not crystallisation ages that would date the fabric formation. If

the muscovite reflects cooling ages then the younger ages closer to the fault indicate that rates of exhumation increase toward the fault.

Alternatively the samples nearest the fault may contain muscovite that grew below the closure temperature of argon in muscovite. This is supported by the observation that the older samples are from the mylonites, whereas the younger muscovite sample closer to the fault was from a C-S fabric phyllite with prominent muscovite growth along the C planes. The growth of muscovite along the C planes deforming the fabric, suggest a portion of syn kinematic fabric formation within the Alpine Schist.

This interpretation of non homogenous deformation during uplift relating to partitioning of the strain between materials that were strongly deformed at deeper levels (Toy et al. 2010) can be seen in the distribution of the foliation and age readings. The shallower foliation readings associated with sample 9, (Figure 3) and older age may be a passive marker uplifted segment that has been sheared, faulted or folded from formation at depth in the shallow ramp of the Alpine Fault (Mortimer 1993).

The older ages away from the Alpine fault indicate that there was earlier cooling of the units east of the Alpine Fault. This later stage cooling closer to the Alpine Fault is indicative of the unit undergoing sustained higher temperature conditions possibly as a result of the inclusion of minor frictional heating related to uplift along the Alpine Fault (Shi et al. 1996), or more likely are a reflection of uplift and exhumation focussed at the Alpine Fault (Little et al. 2002). Work studying quartz fabric within the Alpine Schist exposed in Hare Mare and Gaunt Creek by Toy et al. (2008), indicated that with progression from the Alpine Fault east ward there was a decrease in the preferred orientation of quartz fabrics. The quartz fabrics progressed from prominent asymmetric patterns in line with the Alpine Fault to cross girdle patterns indicating that the strain acting within the region was higher closer to the fault. Not all quartz sampled by Toy et al. (2010) displayed the development of ongoing microstructural

features after emplacement indicating that within the mylonite zone there was not a continuous homogenous deformation during exhumation, suggesting that strain and exhumation are focussed closer to the fault.

## CONCLUSIONS

- Maximum depositional age of Alpine Schist protolith occurred in the Triassic.
- Similarity in detrital zircon populations of Rakaia Terrane and Alpine Schist samples suggests that the Alpine Schist is a metamorphosed section of the Rakaia Terrane.
- The young $^{40}Ar/^{39}Ar$ ages of muscovite with crystallisation along C planes in the Alpine Schist indicate a Pleistocene age of fabric formation not only a Pleistocene age of cooling.
- Younger ages of muscovite toward the Alpine fault indicate that uplift along the fault focuses strain and exhumation closer to the fault with inhomogeneous strain partitioning through the Alpine Schist.

## ACKNOWLEDGMENTS

Thanks go to Adelaide Microscopy for assistance with analytical work, especially to Benjamin Wade (SEM) and Aoife McFadden (LA-ICP-MS). Katie Howard for assistance with Mineral Lab training and James Acott for both his assistance and discussion in the field area and with zircon mount preparation and data analysis. Lastly, I thank my supervisor Alan Collins for his support and discussion throughout the course of the project.

## REFERENCES

ACOTT J. 2013 Honours Thesis, New Zealand where did it come from? Provenace of the Rakaia Terrane. The University of Adelaide.

ADAMS C. J., CAMPBELL H. J. & GRIFFIN W. L. 2007 Provenance comparison of Permian to Jurassic tectonostratigraphic terranes in New Zealand: perspectives from detrital zircon age patterns, *Geology Magazine*, vol. 144, no. 4, pp. 701-729.

COOPER A. F. 1980 Retrograde alteration of chromian kyanite in metachert and amphibolite whiteschist from the Southern Alps, New Zealand, with implications for uplift on the Alpine Fault, *Contributioms to Mineralogy and Petrology*, vol. 75, pp. 153-164.

COOPER A. F., *et al.* 1987 Lamprophyre dike intrusion and the age of the Alpine Fault, New Zealand, *Geology*, vol. 15, pp. 941-944.

CORFU F., *et al.* 2003 Atlas of Zircon Textures. In HANCHAR J. M. & HOSKIN P. W. O. eds. Zircon, Reviews in Mineralogy & Geochemistry. pp. 470-500. Washington, D.C.: Mineralogical Society of America & Geochemical Society.

COX S. & BARRELL D. J. A. 2007 Geology of the Aorakai area. Institute of Geological and Nuclear Sciences 1:250 000 geological map 15.1 sheet + 71 p. Lower Hutt, New Zealand. GNS Science.

CRAW D. 1992 Fluid evolution, fluid immiscibility and gold deposition during Cretaceous-Recent tectonics and uplift of the Otago and Alpine Schist, New Zealand, *Chemical Geology,* vol. 98, pp. 221-236.

DAVEY F., *et al.* 1995 Crustal reflections from the Alpine Fault zone, South Island, New Zealand, *New Zealand Journal of Geology and Geophysics,* vol. 38, pp. 601-604.

GIBSON G. M. & IRELAND T. 1996 Extension of Delamerian (Ross) orogen into western New Zealand: Evidence from zircon ages and implications for crustal growth along the Pacific margin of Gondwana, *Geology,* vol. 24, no. 12, pp. 1087-1090.

GRAPES R. 1995 Uplift and exhumation of Alpine Schist, Southern Alps, New Zealand: thermobarometric constraints, *New Zealand Journal of Geology and Geophysics,* vol. 38, pp. 525-533.

INGHAM M. 1996 Magnetotelluric soundings across the Southern Alps orogen, South Island of New Zealand: data presentation and preliminary interpretation, *Physics of the Earth and Planetray Interiors,* vol. 94, pp. 291-306.

JACKSON S. E., *et al.* 2004 The application of laser ablation-inductively coupled plasma-mass spectrometry to in situ U-Pb zircon geochronology, *Chemical Geology,* vol. 211, pp. 47-69.

JOURDAN F. & RENNE P. R. 2007 Age calibration of the Fish Canyon sanidine $^{40}Ar/^{39}Ar$ dating standard using primary K-Ar standards., *Geochimica et Cosmochimca Acta,* vol. 71, pp. 387-402.

KOPPERS A. A. P. 2002 ArArCALC-software for $^{40}Ar/^{39}Ar$ age calculations, *Computers & Geosciences,* vol. 28, pp. 605-619.

LEE J. Y., *et al.* 2006 A redertimination of the isotopic abundances of atmospheric Ar, *Geochimica et Cosmochimca Acta,* vol. 70, pp. 4507-4512.

LITTLE T. A., *et al.* 2005 Variations in exhumation level and uplift along the oblique-slip Alpine fault, central Southern Alps, New Zealand, *Geological Society of America Bulletin,* vol. 117, no. 5/6, pp. 707-723.

LITTLE T. A., HOLCOMBE R. J. & ILG B. R. 2002 Ductile fabrics in the zone of active oblique convergence near the Alpine Fault, New Zealand: identifying the neotectonic overprint, *Journal of Structural Geology,* vol. 24, no. 1, pp. 193-217.

LITTLE T. A., MORTIMER N. & MCWILLIAMS M. 1999 An episodic Cretaceous cooling model for the Otago-Marlborough Schist, New Zealand, based on 40Ar/39Ar white mica ages, *New Zealand Journal of Geology and Geophysics,* vol. 42, no. 3, pp. 305-325.

MATTINSON J. M., KIMBROUGH D. L. & BRADSHAW J. Y. 1986 Western Fiordland orthogneiss: Early Cretaceous arc magmatism and granulite facies metamorphism, New Zealand, *Contributioms to Mineralogy and Petrology,* vol. 92, pp. 383-392.

MORTIMER N. 1993 Jurassic tectonic history of the Otago Schist, New Zealand, *Tectonics,* vol. 12, pp. 237-244.

MORTIMER N. & COOPER A. F. 2004 U-Pb and Sm-Nd ages from the Alpine Schist, New Zealand, *New Zealand Journal of Geology and Geophysics,* vol. 47, pp. 21-28.

NORRIS J. & COOPER A. F. 1995 Origin of small-scale segmentation and transpressional thrusting along the Alpine fault, New Zealand, *Geological Society of America Bulletin,* vol. 107, no. 2, pp. 231-240.

--- 1997 Erosional control on the structural evolution of a transpressional thrust complex on the Alpine Fault, New Zealand, *Journal of Structural Geology,* vol. 19, no. 10, pp. 1323-1342.

NORRIS R. J. & COOPER A. F. 2000 Late Quaternary slip rates and slip partitioning on the Alpine fault, New Zealand., *Journal of Structural Geology,* vol. 23, pp. 507-520.

PAYNE J. L., *et al.* 2008 Temporal constraints in the timing of high-grade metamorphism in the northern Gawler Craton: Implications for assembly of the Australian Proterozoic, *Australian Journal of Earth Sciences,* vol. 55, pp. 623-640.

PERCIVAL I. G. & GLEN R. A. 2007 Ordovician to earliest Silurian history of the Macquarie Arc, Lachlan Orogen, New South Wales, *Australian Journal of Earth Sciences,* vol. 54, no. 2/3, pp. 143-165.

PICKARD A. L., ADAMS C. J. & BARLEY M. E. 2000 Australian provenance for Upper Permian to Cretaceous rocks forming accretionary complexes on the New Zealand sector of the Gondwanaland Margin, *Australian Journal of Earth Sciences,* vol. 47, pp. 987-1007.

RENNE P. R., *et al.* 2010 Joint determination of $^{40}K$ decay constants and $^{40}Ar^*/^{40}K$ for the Fish Canyon sanidine standard, and improved accuracy for $^{40}Ar/^{39}Ar$ geochronology, *Geochimica et Cosmochimca Acta,* vol. 74, no. 5349-5367.

SHI Y., ALLIS R. & DAVEY F. 1996 Thermal modeling of the Southern Alps, New Zealand, *Pure and Applied Geophysics,* vol. 146, no. 3-4, pp. 469-501.

SIBSON R. H., WHITE S. H. & ATKINSON B. K. 1981 Structure and distribution of fault rocks in the Alpine Fault Zone, New Zealand, *Geological Scoiety of London Special Publication,* vol. 9, pp. 197-210.

SLÁMA J., *et al.* 2008 Plešovice zircon; a new natural reference material for U/Pb and Hf isotopic microanalysis, *Chemical Geology,* vol. 249, no. 1-2, pp. 1-35.

TIMMS N. E., KINNY P. D. & REDDY S. M. 2006 Enhanced diffusion of Uranium and Thorium linked to Crystal plasticity in zircon, *Geochemical Transactions,* vol. 7, no. 10, pp. 1-16.

TOY V. G., *et al.* 2010 Thermal regime in the central Alpine Fault zone, New Zealand: Constraints from microstructures, biotite chemistry and fluid inclusion data, *Tectonophysics,* vol. 485, pp. 178-192.

TOY V. G., PRIOR D. J. & NORRIS J. 2008 Quartz fabrics in the Alpine Fault mylonites: Influence of pre-existing preferred orientations on fabric developments during progressive uplift, *Jounral of Structural Geology,* vol. 30, pp. 602-621.

VERMEESCH P. 2012 On the visualisation of detrital age distributions, *Chemical Geology,* vol. 312-313, pp. 190-194.

VOS I. M. A., BIERLEIN F. B. & WEBB J. 2006 Geochemistry of Early-Middle Palaezoic basalts in the Hodgkinsons Province: a key to tectono-magmatic evolution of the Tasman Fold Belt System in northestern Queensland, Australia, *International Journal of Earth Sciences,* vol. 95, no. 4, pp. 569-585.

VRY J. K., *et al.* 2004 Zoned (Cretaceous and Cenozoic) garnet and the timing of high grade metamorphism, Southern Alps, New Zealand, *Journal of Metamorphic Geology,* vol. 22, pp. 137-157.

VRY J. K., POWELL R. & WILLAIMS J. 2008 Establishing the P-T paths for Alpine Schist, Southern Alps near Hokitika, New Zealand, *Journal of Metamorphic Geology,* vol. 26, pp. 81-97.

WANDRES A. M., *et al.* 2004 Provenance of the sedimentary Rakaia sub-terrane, Torlesse Terrane, South Island, New Zealand: the use of igneous clast compositions to define the source, *Sedimentary Geology,* vol. 168, pp. 193-226.

WANNAMAKER P. E., *et al.* 2002 Fluid generation and pathways beneath an active compressional orogen, the New Zealand Southern Alps, inferred from magnetotelluric data, *Journal of Geophysics Research,* vol. 107, no. B6, pp. 1-21.

WITHNALL I. W., MACKENZIE D. E. & DENARO T. J. 1997 Georgetown Region. In BAIN J. H. C. & DRAPER J. J. eds. North Queensland Geology. pp. 19-116. Australian Geological Survey Organisation.

## APPENDIX

**Supplementary Table 1 Complete Laser Ablation Inductively Coupled Mass Spectrometry Data for Alpine Schist Zircon**

| Analysis | | | | | | | Pb207/Pb206 | | Pb206/U238 | | Pb207/U235 | |
|---|---|---|---|---|---|---|---|---|---|---|---|---|
| | Pb207/U235 | Sigma 1 | Pb206/U238 | Sigma 1 | rho | Concordancy | Age (Ma) | Sigma 1 | Age (Ma) | Sigma 1 | Age (Ma) | Sigma 1 |
| 2_9_3 | 0.34127 | 0.00616 | 0.04509 | 0.00062 | 0.761779 | 95 | 408.5 | 35.96 | 284.3 | 3.84 | 298.1 | 4.66 |
| 2_9_3B | 0.43601 | 0.00809 | 0.04779 | 0.00067 | 0.755589 | 82 | 812.4 | 35.31 | 300.9 | 4.1 | 367.4 | 5.72 |
| 2_9_2A | 0.58718 | 0.00986 | 0.07564 | 0.00106 | 0.834543 | 100 | 464.2 | 31.88 | 470.1 | 6.36 | 469.1 | 6.31 |
| 2_9_2B | 0.5321 | 0.0083 | 0.06759 | 0.00092 | 0.872611 | 97 | 495.2 | 29.21 | 421.6 | 5.55 | 433.2 | 5.5 |
| 2_9_2C | 0.41362 | 0.01356 | 0.05173 | 0.00085 | 0.501208 | 92 | 529.1 | 70.95 | 325.1 | 5.24 | 351.5 | 9.74 |
| 2_9_2D | 0.50665 | 0.01766 | 0.06192 | 0.00105 | 0.486492 | 93 | 581.1 | 75.27 | 387.3 | 6.36 | 416.2 | 11.9 |
| 2_9_1A | 0.34321 | 0.00555 | 0.0421 | 0.00056 | 0.82257 | 89 | 572 | 30.8 | 265.9 | 3.49 | 299.6 | 4.19 |
| 2_9_1B | 0.43416 | 0.00911 | 0.04524 | 0.00065 | 0.684734 | 78 | 916.7 | 40.5 | 285.2 | 4.01 | 366.1 | 6.45 |
| 2_9_4A | 0.25998 | 0.00581 | 0.03544 | 0.0005 | 0.631306 | 96 | 337.8 | 48.09 | 224.5 | 3.12 | 234.6 | 4.68 |
| 2_9_4B | 0.29818 | 0.00839 | 0.03286 | 0.00052 | 0.562409 | 79 | 800.4 | 57.59 | 208.5 | 3.26 | 265 | 6.57 |
| 2_9_4C | 0.24257 | 0.00755 | 0.03468 | 0.00054 | 0.50027 | 100 | 229.2 | 70.96 | 219.8 | 3.39 | 220.5 | 6.17 |
| 2_9_5A | 0.32509 | 0.00595 | 0.04366 | 0.0006 | 0.750852 | 96 | 371 | 37.43 | 275.5 | 3.7 | 285.8 | 4.56 |
| 2_9_6A | 0.27297 | 0.00559 | 0.03626 | 0.00051 | 0.686824 | 94 | 395.2 | 42.31 | 229.6 | 3.2 | 245.1 | 4.46 |
| 2_9_6B | 0.2505 | 0.00539 | 0.03517 | 0.00049 | 0.647504 | 98 | 270.2 | 46.54 | 222.8 | 3.08 | 227 | 4.38 |
| 2_10_1A | 0.15322 | 0.00639 | 0.0204 | 0.00034 | 0.399635 | 90 | 390.9 | 91.29 | 130.2 | 2.16 | 144.8 | 5.63 |
| 2_10_1B | 0.37596 | 0.01319 | 0.02123 | 0.00042 | 0.563892 | 42 | 2076.6 | 64.08 | 135.4 | 2.63 | 324.1 | 9.74 |
| 2_10_2A | 0.32154 | 0.02197 | 0.0328 | 0.00072 | 0.321265 | 74 | 959.9 | 136.78 | 208.1 | 4.5 | 283.1 | 16.88 |
| 2_10_3A | 1.00125 | 0.02343 | 0.03836 | 0.00062 | 0.69069 | 34 | 2735.2 | 39.03 | 242.7 | 3.88 | 704.4 | 11.89 |
| 2_10_4A | 0.29692 | 0.00842 | 0.04098 | 0.00062 | 0.533516 | 98 | 308.6 | 62.49 | 258.9 | 3.82 | 264 | 6.59 |
| 2_10_4B | 0.57149 | 0.02618 | 0.04337 | 0.00088 | 0.442927 | 60 | 1539 | 86.72 | 273.7 | 5.42 | 459 | 16.91 |
| 2_10_5A | 0.14637 | 0.00332 | 0.01984 | 0.00028 | 0.6222 | 91 | 349.3 | 49.07 | 126.6 | 1.78 | 138.7 | 2.94 |
| 2_10_2B | 0.56133 | 0.01837 | 0.03323 | 0.00062 | 0.570125 | 47 | 1993.1 | 59.94 | 210.7 | 3.87 | 452.4 | 11.95 |
| 2_10_2C | 0.27332 | 0.01139 | 0.03245 | 0.00057 | 0.42151 | 84 | 642.5 | 89.04 | 205.9 | 3.58 | 245.3 | 9.08 |
| 2_10_3B | 0.29188 | 0.00894 | 0.03586 | 0.00057 | 0.518957 | 87 | 568.4 | 65.95 | 227.1 | 3.53 | 260 | 7.03 |
| 2_10_5B | 0.32997 | 0.00678 | 0.02141 | 0.00032 | 0.727408 | 47 | 1828.9 | 36.27 | 136.5 | 1.99 | 289.5 | 5.18 |
| 2_10_5C | 0.14014 | 0.00314 | 0.01952 | 0.00028 | 0.640193 | 94 | 288 | 48.97 | 124.6 | 1.75 | 133.2 | 2.8 |
| 2_10_5D | 0.18874 | 0.00765 | 0.01969 | 0.00037 | 0.463616 | 72 | 914.1 | 84.01 | 125.7 | 2.32 | 175.6 | 6.53 |
| 2_10_6A | 0.28274 | 0.0081 | 0.03903 | 0.00059 | 0.527662 | 98 | 309.2 | 63.78 | 246.8 | 3.66 | 252.8 | 6.41 |
| 2_10_6B | 0.28496 | 0.00668 | 0.03709 | 0.00053 | 0.609574 | 92 | 441.3 | 49.94 | 234.7 | 3.3 | 254.6 | 5.28 |
| 2_10_6C | 0.30555 | 0.00651 | 0.03881 | 0.00054 | 0.653057 | 91 | 495.2 | 44.56 | 245.4 | 3.37 | 270.7 | 5.06 |

| | | | | | | | | | | | | |
|---|---|---|---|---|---|---|---|---|---|---|---|---|
| 2_10_7A | 0.19605 | 0.00588 | 0.02168 | 0.00035 | 0.538268 | 76 | 793.1 | 62.52 | 138.3 | 2.18 | 181.8 | 4.99 |
| 2_10_7B | 0.25103 | 0.0352 | 0.02244 | 0.00118 | 0.375009 | 63 | 1225 | 267.44 | 143 | 7.42 | 227.4 | 28.57 |
| 2_10_7C | 0.15024 | 0.00262 | 0.02053 | 0.00027 | 0.754152 | 92 | 332.4 | 35.85 | 131 | 1.73 | 142.1 | 2.31 |
| 2_10_8A | 0.32262 | 0.00914 | 0.04311 | 0.00065 | 0.532207 | 96 | 382.4 | 62.36 | 272.1 | 4.04 | 283.9 | 7.02 |
| 2_10_8B | 0.33309 | 0.00738 | 0.0411 | 0.00058 | 0.63693 | 89 | 559.2 | 46.35 | 259.6 | 3.59 | 291.9 | 5.62 |
| 2_10_9A | 0.28984 | 0.00747 | 0.0398 | 0.00058 | 0.565435 | 97 | 320.9 | 56.94 | 251.6 | 3.61 | 258.4 | 5.88 |
| 2_10_9B | 0.28669 | 0.00864 | 0.03894 | 0.0006 | 0.511274 | 96 | 345.8 | 67.3 | 246.3 | 3.74 | 256 | 6.82 |
| 2_10_9C | 0.27476 | 0.00522 | 0.03813 | 0.00052 | 0.717827 | 98 | 296.9 | 40.35 | 241.3 | 3.2 | 246.5 | 4.16 |
| 2_10_10A | 0.38349 | 0.00786 | 0.04778 | 0.00066 | 0.673952 | 91 | 537.6 | 43.14 | 300.9 | 4.06 | 329.6 | 5.77 |
| 2_10_10B | 0.27976 | 0.00502 | 0.03905 | 0.00052 | 0.742103 | 99 | 284.1 | 37.75 | 246.9 | 3.24 | 250.5 | 3.98 |
| 2_10_10C | 0.27418 | 0.00553 | 0.03785 | 0.00052 | 0.681158 | 97 | 309.2 | 43.37 | 239.5 | 3.22 | 246 | 4.41 |
| 2_10_11A | 0.27952 | 0.00848 | 0.03414 | 0.00052 | 0.802186 | 86 | 581.8 | 65.08 | 216.4 | 3.26 | 250.3 | 6.73 |
| 2_10_11B | 0.2575 | 0.00838 | 0.03449 | 0.00053 | 0.802186 | 94 | 377.3 | 72.04 | 218.6 | 3.31 | 232.7 | 6.77 |
| 2_10_11C | 0.23319 | 0.00962 | 0.03217 | 0.00057 | 0.802186 | 96 | 310.4 | 93.57 | 204.1 | 3.54 | 212.8 | 7.92 |
| 2_10_12A | 0.31043 | 0.00768 | 0.04257 | 0.0006 | 0.802186 | 98 | 324.4 | 54.43 | 268.7 | 3.71 | 274.5 | 5.95 |
| 2_10_12B | 0.31713 | 0.01667 | 0.03886 | 0.00082 | 0.802186 | 88 | 574.4 | 114.52 | 245.8 | 5.09 | 279.7 | 12.85 |
| 2_10_12C | 0.41522 | 0.0117 | 0.04066 | 0.00063 | 0.802186 | 73 | 1043.4 | 56.69 | 256.9 | 3.89 | 352.6 | 8.4 |
| 2_10_13A | 0.3068 | 0.00796 | 0.04022 | 0.00058 | 0.802186 | 94 | 425.5 | 56.34 | 254.2 | 3.61 | 271.7 | 6.18 |
| 2_10_13B | 0.30482 | 0.00618 | 0.03945 | 0.00053 | 0.802186 | 92 | 454 | 42.81 | 249.4 | 3.3 | 270.2 | 4.81 |
| 2_10_13C | 0.33439 | 0.00963 | 0.04026 | 0.00061 | 0.802186 | 87 | 612.2 | 61.89 | 254.5 | 3.81 | 292.9 | 7.33 |
| 2_10_14A | 0.15519 | 0.01061 | 0.01865 | 0.00046 | 0.802186 | 81 | 616.3 | 146.63 | 119.1 | 2.9 | 146.5 | 9.33 |
| 2_10_14B | 0.17186 | 0.00522 | 0.01946 | 0.0003 | 0.802186 | 77 | 743.2 | 64.04 | 124.3 | 1.9 | 161 | 4.52 |
| 2_10_14C | 0.1615 | 0.00811 | 0.02017 | 0.00039 | 0.802186 | 85 | 532.3 | 110.13 | 128.7 | 2.46 | 152 | 7.09 |
| 2_10_15A | 0.17694 | 0.00572 | 0.0239 | 0.00037 | 0.802186 | 92 | 358.5 | 72.29 | 152.2 | 2.31 | 165.4 | 4.93 |
| 2_10_15B | 0.24336 | 0.00598 | 0.02381 | 0.00035 | 0.802186 | 69 | 1045.4 | 49.2 | 151.7 | 2.17 | 221.2 | 4.88 |
| 2_10_15C | 0.87151 | 0.03387 | 0.025 | 0.00069 | 0.802186 | 25 | 3202.9 | 69.98 | 159.2 | 4.36 | 636.4 | 18.38 |
| 2_10_15D | 0.23448 | 0.00531 | 0.02426 | 0.00034 | 0.802186 | 72 | 931.3 | 45.76 | 154.5 | 2.13 | 213.9 | 4.37 |
| 2_10_16A | 0.36984 | 0.01555 | 0.04551 | 0.00083 | 0.802186 | 90 | 565.1 | 92.04 | 286.9 | 5.09 | 319.5 | 11.53 |
| 2_10_16B | 0.51371 | 0.0137 | 0.04967 | 0.00074 | 0.802186 | 74 | 1069 | 53.75 | 312.5 | 4.57 | 420.9 | 9.19 |
| 2_10_16C | 0.54449 | 0.04447 | 0.04374 | 0.00147 | 0.802186 | 63 | 1431.8 | 157.33 | 276 | 9.07 | 441.4 | 29.23 |
| 2_10_17A | 0.14505 | 0.01018 | 0.02181 | 0.00053 | 0.775336 | 101 | 111.7 | 163.07 | 139.1 | 3.32 | 137.5 | 9.03 |
| 2_10_17B | 0.2269 | 0.01501 | 0.01955 | 0.00051 | 0.775336 | 60 | 1296.6 | 129.46 | 124.8 | 3.23 | 207.6 | 12.42 |
| 2_10_18A | 0.4079 | 0.00802 | 0.03705 | 0.00051 | 0.775336 | 68 | 1193.4 | 37.22 | 234.6 | 3.18 | 347.4 | 5.78 |

| | | | | | | | | | | | | |
|---|---|---|---|---|---|---|---|---|---|---|---|---|
| 2_10_18B | 0.29738 | 0.00858 | 0.03569 | 0.00054 | 0.775336 | 86 | 619.6 | 61.52 | 226.1 | 3.35 | 264.4 | 6.71 |
| 2_10_19A | 0.19048 | 0.0083 | 0.02592 | 0.00045 | 0.775336 | 93 | 342.2 | 97.52 | 164.9 | 2.83 | 177 | 7.08 |
| 2_10_19B | 0.19374 | 0.00947 | 0.02633 | 0.00051 | 0.775336 | 93 | 345.1 | 110 | 167.5 | 3.19 | 179.8 | 8.06 |
| 2_10_20A | 0.14487 | 0.00269 | 0.0218 | 0.00029 | 0.775336 | 101 | 109.9 | 41.2 | 139 | 1.82 | 137.4 | 2.39 |
| 2_10_20B | 0.17104 | 0.00451 | 0.02223 | 0.00032 | 0.775336 | 88 | 444.5 | 57.53 | 141.7 | 2.03 | 160.3 | 3.91 |
| 2_10_21A | 0.25801 | 0.00473 | 0.03539 | 0.00047 | 0.775336 | 96 | 324.1 | 39.04 | 224.2 | 2.91 | 233.1 | 3.82 |
| 2_10_21B | 0.26201 | 0.01237 | 0.03401 | 0.00066 | 0.775336 | 91 | 447.6 | 105.44 | 215.6 | 4.13 | 236.3 | 9.95 |
| 2_10_22A | 0.30884 | 0.00769 | 0.04061 | 0.00058 | 0.775336 | 94 | 418.6 | 54.01 | 256.6 | 3.6 | 273.3 | 5.97 |
| 2_10_22B | 0.27688 | 0.00489 | 0.03966 | 0.00052 | 0.775336 | 101 | 224.5 | 38.19 | 250.7 | 3.22 | 248.2 | 3.89 |
| 2_10_22C | 0.26845 | 0.00505 | 0.03704 | 0.00049 | 0.775336 | 97 | 310.4 | 40.58 | 234.5 | 3.05 | 241.5 | 4.05 |
| 2_10_23A | 0.23102 | 0.01074 | 0.03004 | 0.00057 | 0.775336 | 90 | 443.1 | 103.82 | 190.8 | 3.58 | 211 | 8.86 |
| 2_10_23B | 0.30819 | 0.00588 | 0.03075 | 0.00041 | 0.775336 | 72 | 1005.7 | 37.14 | 195.2 | 2.59 | 272.8 | 4.56 |
| 2_10_24A | 28.49028 | 0.45721 | 0.68026 | 0.00883 | 0.775336 | 97 | 3489.6 | 22.94 | 3345.4 | 33.87 | 3436.1 | 15.74 |
| 2_10_24B | 28.25982 | 0.43739 | 0.65591 | 0.00871 | 0.578706 | 95 | 3533.7 | 20.92 | 3251.3 | 33.89 | 3428.2 | 15.18 |
| 2_10_24C | 6.4113 | 0.5674 | 0.21226 | 0.01311 | 0.578706 | 61 | 2974.4 | 155.33 | 1240.9 | 69.69 | 2033.8 | 77.74 |
| 2_10_25A | 1.02244 | 0.018 | 0.11179 | 0.00151 | 0.578706 | 96 | 817.5 | 33.79 | 683.1 | 8.78 | 715.1 | 9.04 |
| 2_10_25B | 0.61898 | 0.07555 | 0.06056 | 0.00293 | 0.578706 | 77 | 1045.6 | 241.42 | 379 | 17.8 | 489.2 | 47.38 |
| 2_10_26A | 0.30809 | 0.01584 | 0.03772 | 0.00078 | 0.578706 | 88 | 576.7 | 111.77 | 238.7 | 4.87 | 272.7 | 12.3 |
| 2_10_26B | 0.28971 | 0.00907 | 0.03768 | 0.00059 | 0.578706 | 92 | 443.2 | 68.96 | 238.4 | 3.69 | 258.3 | 7.14 |
| 2_10_26C | 0.27654 | 0.01165 | 0.03775 | 0.00066 | 0.578706 | 96 | 334.9 | 94.46 | 238.9 | 4.08 | 247.9 | 9.27 |
| 2_10_27A | 0.37777 | 0.01764 | 0.02994 | 0.00064 | 0.578706 | 58 | 1457.8 | 90.57 | 190.2 | 3.99 | 325.4 | 13 |
| 2_10_27B | 0.36985 | 0.0149 | 0.02972 | 0.00058 | 0.578706 | 59 | 1431.4 | 78.48 | 188.8 | 3.63 | 319.5 | 11.04 |
| 2_10_27C | 0.28916 | 0.01174 | 0.02859 | 0.00053 | 0.578706 | 70 | 1024.4 | 82.77 | 181.7 | 3.31 | 257.9 | 9.24 |
| 2_10_28A | 0.29375 | 0.00771 | 0.03783 | 0.00056 | 0.578706 | 92 | 464.5 | 57.86 | 239.4 | 3.49 | 261.5 | 6.05 |
| 2_10_28B | 0.40166 | 0.01438 | 0.0378 | 0.00068 | 0.578706 | 70 | 1123.4 | 72.49 | 239.2 | 4.23 | 342.9 | 10.42 |
| 2_10_28C | 0.91281 | 0.05 | 0.03028 | 0.0011 | 0.578706 | 29 | 2971 | 98.95 | 192.3 | 6.85 | 658.6 | 26.54 |
| 2_10_30A | 0.53917 | 0.01089 | 0.0699 | 0.00096 | 0.578706 | 99 | 450.1 | 42.81 | 435.6 | 5.78 | 437.9 | 7.18 |
| 2_10_30B | 0.55495 | 0.01069 | 0.06996 | 0.00095 | 0.578706 | 97 | 512.1 | 40.81 | 435.9 | 5.72 | 448.2 | 6.98 |
| 2_10_29A | 0.28063 | 0.00768 | 0.03677 | 0.00055 | 0.578706 | 93 | 426.7 | 60.18 | 232.8 | 3.43 | 251.2 | 6.09 |
| 2_10_29B | 0.25091 | 0.00579 | 0.03458 | 0.00049 | 0.578706 | 96 | 313.2 | 51.35 | 219.1 | 3.04 | 227.3 | 4.7 |
| 2_10_29C | 0.30739 | 0.00932 | 0.03397 | 0.00054 | 0.578706 | 79 | 794.9 | 63.84 | 215.3 | 3.36 | 272.2 | 7.24 |
| 2_10_31A | 0.31828 | 0.00653 | 0.04345 | 0.0006 | 0.794962 | 98 | 333.1 | 44.09 | 274.2 | 3.7 | 280.6 | 5.03 |
| 2_10_31B | 0.36934 | 0.01073 | 0.04355 | 0.00068 | 0.794962 | 86 | 656.2 | 61.88 | 274.8 | 4.21 | 319.2 | 7.95 |

| | | | | | | | | | | | | |
|---|---|---|---|---|---|---|---|---|---|---|---|---|
| 2_10_32A | 0.28116 | 0.00493 | 0.03842 | 0.00051 | 0.794962 | 97 | 330.8 | 36.57 | 243.1 | 3.17 | 251.6 | 3.91 |
| 2_10_32B | 0.44746 | 0.01151 | 0.03833 | 0.00059 | 0.794962 | 65 | 1307 | 49.89 | 242.5 | 3.67 | 375.5 | 8.08 |
| 2_10_33A | 0.21654 | 0.006 | 0.02934 | 0.00044 | 0.794962 | 94 | 350.5 | 61.78 | 186.4 | 2.76 | 199 | 5 |
| 2_10_33B | 0.20086 | 0.0043 | 0.02952 | 0.00041 | 0.794962 | 101 | 163.5 | 47.98 | 187.5 | 2.55 | 185.9 | 3.64 |
| 2_10_33C | 0.23183 | 0.00795 | 0.03035 | 0.00049 | 0.794962 | 91 | 427 | 75.76 | 192.8 | 3.06 | 211.7 | 6.55 |
| 2_10_34A | 0.21035 | 0.00567 | 0.02523 | 0.00038 | 0.794962 | 83 | 619.9 | 57.54 | 160.6 | 2.39 | 193.8 | 4.75 |
| 2_10_34B | 0.22383 | 0.00589 | 0.0266 | 0.00039 | 0.794962 | 82 | 639.2 | 55.81 | 169.2 | 2.46 | 205.1 | 4.89 |
| 2_15_01A | 0.27857 | 0.00882 | 0.03936 | 0.0006 | 0.794962 | 100 | 254.6 | 71.81 | 248.9 | 3.72 | 249.5 | 7.01 |
| 2_15_01B | 0.28797 | 0.00677 | 0.03562 | 0.0005 | 0.794962 | 88 | 552.5 | 49.96 | 225.7 | 3.13 | 257 | 5.33 |
| 2_15_03A | 0.15218 | 0.00594 | 0.01994 | 0.00033 | 0.794962 | 89 | 425.3 | 86.25 | 127.3 | 2.08 | 143.8 | 5.23 |
| 2_15_03B | 0.18674 | 0.0089 | 0.02059 | 0.0004 | 0.794962 | 76 | 798.2 | 100.32 | 131.4 | 2.55 | 173.8 | 7.61 |
| 2_15_4A | 0.32562 | 0.00895 | 0.04313 | 0.00064 | 0.650285 | 95 | 403.4 | 59.43 | 272.2 | 3.94 | 286.2 | 6.85 |
| 2_15_4B | 0.29483 | 0.00811 | 0.04211 | 0.00063 | 0.650285 | 101 | 231.8 | 62.25 | 265.9 | 3.89 | 262.4 | 6.36 |
| 2_15_4C | 0.36269 | 0.0114 | 0.03882 | 0.00064 | 0.650285 | 78 | 861.9 | 65.24 | 245.5 | 3.94 | 314.2 | 8.5 |
| 2_15_5A | 0.28281 | 0.02452 | 0.02108 | 0.0007 | 0.650285 | 53 | 1574 | 162.3 | 134.4 | 4.43 | 252.9 | 19.41 |
| 2_15_5B | 0.60049 | 0.02077 | 0.02124 | 0.00047 | 0.650285 | 28 | 2866.9 | 60.74 | 135.5 | 2.96 | 477.5 | 13.17 |
| 2_15_5C | 0.40002 | 0.03167 | 0.02202 | 0.00069 | 0.650285 | 41 | 2122.1 | 139.63 | 140.4 | 4.32 | 341.7 | 22.97 |
| 2_15_6A | 0.1709 | 0.00679 | 0.01945 | 0.00033 | 0.650285 | 78 | 733.4 | 83.9 | 124.2 | 2.11 | 160.2 | 5.89 |
| 2_15_6B | 0.2323 | 0.02006 | 0.01851 | 0.00066 | 0.650285 | 56 | 1446.9 | 165.88 | 118.2 | 4.15 | 212.1 | 16.53 |

**Supplementary Table 2 Decimal degrees GPS coordinates of transects**

| Stop | Latitude | Longitude | Transect |
|---|---|---|---|
| 1 | -43.38775 | 170.204194 | Tatare Stream |
| 2 | -43.387944 | 170.204639 | Tatare Stream |
| 3 | -43.387917 | 170.205222 | Tatare Stream |
| 4 | -43.389417 | 170.207 | Tatare Stream |
| 5 | -43.38825 | 170.209028 | Tatare Stream |
| 6 | -43.387167 | 170.204611 | Tatare Stream |
| 7 | -43.416667 | 170.182667 | Waiho River |
| 8 | -43.418861 | 170.180722 | Waiho River |
| 9 | -43.420222 | 170.178833 | Waiho River |
| 10 | -43.422278 | 170.177806 | Waiho River |
| 11 | -43.422583 | 170.177639 | Waiho River |
| 12 | -43.422972 | 170.1775 | Waiho River |
| 13 | -43.423222 | 170.177083 | Waiho River |
| 14 | -43.423972 | 170.176861 | Waiho River |
| 15 | -43.42475 | 170.176889 | Waiho River |
| 16 | -43.4255 | 170.176833 | Waiho River |
| 17 | -43.426083 | 170.176861 | Waiho River |
| 18 | -43.426639 | 170.176417 | Waiho River |
| 19 | -43.427417 | 170.175694 | Waiho River |
| 20 | -43.420194 | 170.178389 | Waiho River |
| 21 | -43.426694 | 170.169694 | Waiho River |
| 22 | -43.303833 | 170.399 | Tommy Creek |
| 23 | -43.304139 | 170.39825 | Tommy Creek |
| 24 | -43.304806 | 170.397417 | Tommy Creek |
| 25 | -43.305806 | 170.396778 | Tommy Creek |
| 26 | -43.303694 | 170.396833 | Tommy Creek |
| 27 | -43.302806 | 170.395833 | Tommy Creek |
| 28 | -43.30275 | 170.394778 | Tommy Creek |
| 29 | -43.30225 | 170.393472 | Tommy Creek |
| 30 | -43.401139 | 170.187278 | Waiho River |
| 31 | -43.439444 | 170.171167 | Waiho River |
| 32 | -43.437333 | 170.170278 | Waiho River |
| 33 | -43.431222 | 170.168528 | Waiho River |
| 34 | -43.441889 | 170.08075 | Hare Mare Creek |
| 35 | [redacted] | [redacted] | Hare Mare Creek |
| 36 | -43.441611 | 170.081972 | Hare Mare Creek |
| 37 | -43.4415 | 170.082361 | Hare Mare Creek |
| 38 | -43.440778 | 170.083194 | Hare Mare Creek |
| 39 | -43.441806 | 170.085639 | Hare Mare Creek |
| 40 | -43.441694 | 170.086139 | Hare Mare Creek |
| 41 | -43.44125 | 170.087222 | Hare Mare Creek |
| 42 | -43.443917 | 170.07025 | Waikukupa River |
| 43 | -43.442917 | 170.070611 | Waikukupa River |
| 44 | -43.441917 | 170.072167 | Waikukupa River |
| 45 | -43.440444 | 170.071806 | Waikukupa River |
| 46 | -43.4395 | 170.071419 | Waikukupa River |

**Supplementary Table 3 Structural measurements taken along Alpine Schist transects**

| Stop | Foliation Dip | Measurements Direction | Lineation Plunge | Measurements Direction |
|---|---|---|---|---|
| 1 | 68 | 143 | 19 | 219 |
| | 61 | 140 | 20 | 214 |
| | 55 | 142 | 31 | 221 |
| | 60 | 148 | | |
| | 60 | 146 | | |
| 2 | 53 | 149 | 29 | 220 |
| | 50 | 152 | 21 | 213 |
| | 52 | 159 | 33 | 218 |
| 3 | 55 | 159 | 33 | 201 |
| 4 | | | | |
| 5 | 69 | 137 | 21 | 229 |
| | 58 | 133 | | |
| | 60 | 133 | 23 | 215 |
| | 70 | 129 | 23 | 213 |
| | 66 | 122 | 32 | 209 |
| 6 | 63 | 136 | 20 | 212 |
| | 67 | 149 | 28 | 216 |
| | 63 | 136 | 30 | 219 |
| | 62 | 148 | 25 | 216 |
| | 67 | 149 | | |
| | 70 | 142 | | |
| 7 | 52 | 130 | | |
| | 45 | 141 | | |
| | 58 | 139 | | |
| | 32 | 133 | | |
| | 52 | 144 | | |
| 8 | 69 | 137 | 34 | 201 |
| | 63 | 133 | 18 | 205 |
| | 64 | 130 | 28 | 202 |
| | 58 | 135 | | |
| | 60 | 133 | | |
| 9 | 70 | 132 | | |
| | 62 | 141 | | |
| | 68 | 133 | | |
| 10 | 67 | 133 | 22 | 186 |
| | 65 | 146 | | |
| | 33 | 147 | | |
| 11 | 38 | 147 | | |
| | 44 | 130 | | |
| | 49 | 142 | | |
| 12 | 80 | 136 | | |
| | 77 | 131 | | |
| | 78 | 128 | | |
| | 62 | 131 | | |
| 13 | 67 | 130 | | |
| | 62 | 131 | | |
| | 42 | 139 | | |
| 14 | 65 | 131 | | |
| 15 | 60 | 134 | 32 | 216 |
| | 62 | 140 | 33 | 218 |
| | 67 | 140 | 24 | 223 |
| | 68 | 133 | | |
| 16 | 67 | 121 | 42 | 210 |
| | 69 | 122 | 31 | 210 |
| | 73 | 122 | | |
| | 68 | 128 | | |
| 17 | 69 | 132 | | |
| | 71 | 129 | | |
| | 67 | 129 | | |
| 18 | 60 | 129 | 22 | 220 |
| | 64 | 135 | 30 | 225 |
| | 73 | 126 | 35 | 223 |
| | 63 | 128 | | |
| 19 | 73 | 128 | 38 | 217 |
| | 72 | 130 | 37 | 213 |
| | 61 | 127 | 33 | 221 |
| | 72 | 123 | 43 | 216 |
| | 80 | 111 | 42 | 211 |
| | 73 | 136 | | |
| | 69 | 120 | | |
| 20 | 67 | 128 | 28 | 225 |
| 21 | 69 | 145 | | |
| | 62 | 155 | | |
| 22 | 80 | 125 | 31 | 209 |
| | 66 | 133 | 30 | 220 |
| | 72 | 127 | 37 | 221 |
| | 69 | 134 | | |
| | 73 | 131 | | |
| | 69 | 131 | | |
| 23 | 54 | 125 | 20 | 208 |
| | 59 | 122 | 23 | 207 |
| | 47 | 131 | | |
| | 49 | 127 | | |
| 24 | 69 | 141 | 32 | 203 |
| | 49 | 139 | | |
| | 43 | 150 | | |
| 25 | 75 | 130 | 28 | 223 |
| | 56 | 119 | | |
| | 57 | 131 | | |

| Stop | Foliation Dip | Measurements Direction | Lineation Plunge | Measurem Direction |
|---|---|---|---|---|
| 26 | 73 | 345 | 40 | 269 |
| | 80 | 349 | 37 | 251 |
| | 84 | 350 | 33 | 252 |
| | 76 | 350 | | |
| | 80 | 342 | | |
| 27 | 71 | 5 | 30 | 269 |
| | 74 | 359 | 39 | 268 |
| | 75 | 352 | | |
| | 71 | 357 | | |
| 28 | 67 | 334 | | |
| | 69 | 340 | | |
| | 70 | 339 | | |
| | 60 | 338 | | |
| | 70 | 336 | | |
| | 64 | 323 | | |
| 29 | 69 | 344 | | |
| | 75 | 341 | | |
| | 71 | 340 | | |
| | 77 | 348 | | |
| 30 | 66 | 125 | 20 | 204 |
| | 65 | 130 | 15 | 201 |
| | 68 | 120 | 21 | 221 |
| | 58 | 132 | | |
| 31 | 72 | 125 | | |
| | 69 | 128 | | |
| | 72 | 125 | | |
| 32 | 67 | 130 | 35 | 212 |
| | 76 | 133 | 41 | 219 |
| | 71 | 129 | 43 | 218 |
| 33 | 80 | 129 | 38 | 212 |
| | 76 | 121 | 41 | 215 |
| | 72 | 120 | 30 | 223 |
| | 72 | 130 | | |
| 34 | 31 | 133 | | |
| | 32 | 141 | | |
| | 31 | 147 | | |
| | 30 | 141 | | |
| | 33 | 138 | | |
| 35 | 35 | 127 | | |
| | 36 | 124 | | |
| | 23 | 123 | | |
| | 40 | 127 | | |
| | 36 | 133 | | |
| 36 | 29 | 114 | 18 | 217 |
| | 26 | 112 | 22 | 216 |
| | 28 | 108 | 23 | 209 |
| | 30 | 121 | | |
| | 31 | 142 | | |
| 37 | 31 | 127 | | |
| | 35 | 130 | | |
| | 41 | 126 | | |
| | 35 | 128 | | |
| 38 | 35 | 148 | | |
| | 34 | 137 | | |
| | 32 | 143 | | |
| | 31 | 139 | | |
| | 32 | 141 | | |
| 39 | 32 | 120 | | |
| | 33 | 128 | | |
| | 30 | 120 | | |
| | 34 | 118 | | |
| | 20 | 120 | | |
| 40 | 23 | 139 | | |
| | 33 | 138 | | |
| | 31 | 135 | | |
| | 29 | 135 | | |
| 41 | 28 | 136 | 4 | 229 |
| | 39 | 127 | | |
| | 36 | 132 | | |
| | 40 | 134 | | |
| | 43 | 130 | | |
| 42 | 23 | 285 | | |
| | 20 | 304 | | |
| 43 | | | | |
| 44 | 13 | 161 | | |
| | 8 | 166 | | |
| | 10 | 150 | | |
| | 12 | 177 | | |
| 45 | 7 | 156 | | |
| | 6 | 153 | | |
| | 32 | 130 | | |
| | 21 | 116 | | |
| 46 | 13 | 163 | | |
| | 17 | 159 | | |
| | 18 | 161 | | |
| | 23 | 153 | | |

## Supplementary Table 4 Sample NZ1306 $^{39}Ar/^{40}Ar$ Analysis

| Relative Abundances | | | 36Ar [V] | %1σ | 37Ar [V] | %1σ | 38Ar [V] | %1σ | 39Ar [V] | %1σ | 40Ar [V] | %1σ | 40(r)/39(k) ± 2σ | Age ± 2σ (Ma) | 40Ar(r) (%) | 39Ar(k) (%) | K/Ca ± 2σ |
|---|---|---|---|---|---|---|---|---|---|---|---|---|---|---|---|---|---|
| 3M30319D | 66 °C | | 0.0000631 | 9.501 | 0.0000082 | 2271.434 | 0.0000341 | 16.114 | 0.0016257 | 0.962 | 0.0187645 | 0.619 | 0.05241 ± 2.20817 | 0.06 ± 2.64 | 0.45 | 1.75 | 85 ± 3867 |
| 3M30320D | 67 °C | | 0.0000574 | 11.023 | 0.0001008 | 171.819 | 0.0000367 | 16.399 | 0.0016199 | 2.202 | 0.0158116 | 0.585 | 0.81776 ± 2.33400 | 0.98 ± 2.79 | 8.38 | 1.75 | 7 ± 24 |
| 3M30322D | 68 °C | 4 | 0.0000724 | 12.635 | 0.0001223 | 158.373 | 0.0000596 | 10.649 | 0.0028787 | 1.308 | 0.0264171 | 0.529 | 1.67548 ± 1.89947 | 2.00 ± 2.27 | 18.26 | 3.11 | 10 ± 32 |
| 3M30323D | 69 °C | 4 | 0.0003774 | 4.352 | 0.0000303 | 656.511 | 0.0004303 | 3.015 | 0.0280895 | 0.482 | 0.1586264 | 0.190 | 1.63480 ± 0.35030 | 1.95 ± 0.42 | 28.95 | 30.32 | 398 ± 5229 |
| 3M30324D | 69 °C | 4 | 0.0001066 | 4.860 | 0.0001523 | 126.547 | 0.0002845 | 3.138 | 0.0197356 | 0.658 | 0.0577010 | 0.266 | 1.31072 ± 0.15853 | 1.57 ± 0.19 | 44.83 | 21.30 | 56 ± 141 |
| 3M30325D | 70 °C | 4 | 0.0001577 | 6.984 | 0.0000598 | 355.577 | 0.0001489 | 9.619 | 0.0092262 | 0.543 | 0.0595022 | 0.229 | 1.34376 ± 0.71383 | 1.61 ± 0.85 | 20.84 | 9.96 | 66 ± 472 |
| 3M30327D | 70 °C | 4 | 0.0001346 | 6.415 | 0.0001262 | 165.806 | 0.0000630 | 10.512 | 0.0033364 | 1.451 | 0.0412858 | 0.328 | 0.32853 ± 1.54736 | 0.39 ± 1.85 | 2.66 | 3.60 | 11 ± 38 |
| 3M30328D | 71 °C | 4 | 0.0001229 | 5.244 | 0.0000974 | 183.555 | 0.0000488 | 14.097 | 0.0022668 | 1.966 | 0.0363589 | 0.386 | 0.15078 ± 1.70249 | 0.18 ± 2.04 | 0.94 | 2.45 | 10 ± 37 |
| 3M30329D | 71 °C | 4 | 0.0001082 | 3.922 | 0.0001625 | 110.557 | 0.0000559 | 9.596 | 0.0024000 | 1.405 | 0.0347490 | 0.499 | 1.01498 ± 1.06622 | 1.21 ± 1.27 | 7.01 | 2.59 | 6 ± 14 |
| 3M30330D | 72 °C | 4 | 0.0001176 | 5.664 | 0.0001634 | 122.245 | 0.0000714 | 10.264 | 0.0035895 | 1.402 | 0.0411858 | 0.323 | 1.68387 ± 1.11225 | 2.01 ± 1.33 | 14.68 | 3.87 | 9 ± 23 |
| 3M30332D | 72 °C | 4 | 0.0000894 | 8.399 | 0.0001885 | 95.971 | 0.0000690 | 11.762 | 0.0038819 | 1.329 | 0.0348837 | 0.374 | 2.10520 ± 1.15845 | 2.51 ± 1.38 | 23.43 | 4.19 | 9 ± 17 |
| 3M30333D | 80 °C | 4 | 0.0001392 | 3.310 | 0.0000264 | 690.151 | 0.0000863 | 8.378 | 0.0050562 | 1.049 | 0.0503220 | 0.340 | 1.73121 ± 0.54987 | 2.07 ± 0.66 | 17.39 | 5.46 | 82 ± 1135 |
| 3M30334D | 82 °C | 4 | 0.0002645 | 3.103 | 0.0000450 | 393.756 | 0.0001662 | 7.387 | 0.0089394 | 0.673 | 0.0943692 | 0.184 | 1.72153 ± 0.55050 | 2.06 ± 0.66 | 16.31 | 9.65 | 85 ± 672 |
| | | Σ | 0.0018111 | 1.657 | 0.0005668 | 120.905 | 0.0015545 | 2.036 | 0.0926458 | 0.259 | 0.6699774 | 0.087 | | | | | |

| Information on Analysis | | |
|---|---|---|
| Sample = NZ1306 | Age Equations = Min et al. (2000) | |
| Material = Msc | Negative Intensities = Allowed | |
| Location = Laser | Decay Constant 40K = 5.531 ± 0.013 E-10 1/a | |
| Analyst = Fred Jourdan | Decay Constant 39Ar = 2.940 ± 0.029 E-07 1/h | |
| Project = ALPINE SHIST_WH13 | Decay Constant 37Ar = 8.230 ± 0.082 E-04 1/h | |
| Mass Discrimination Law = POW | Decay Constant 36Cl = 2.303 ± 0.046 E-06 1/a | |
| Irradiation = I17t3h | Decay Constant 40K(EC,β⁺) = 0.576 ± 0.002 E-10 1/a | |
| J = 0.00066100 ± 0.00000100 | Decay Constant 40K(β⁻) = 4.955 ± 0.013 E-10 1/a | |
| FCs = 28.294 ± 0.037 Ma | Atmospheric Ratio 40/36(a) = 298.56 ± 0.30 | |
| IGSN = Undefined | Atmospheric Ratio 38/36(a) = 0.1869 ± 0.0002 | |
| Preferred Age = Undefined | Production Ratio 39/37(ca) = 0.000706 ± 0.000049 | |
| Classification = Undefined | Production Ratio 38/37(ca) = 0.000023 ± 0.000002 | |
| Experiment Type = Undefined | Production Ratio 36/37(ca) = 0.000281 ± 0.000008 | |
| Extraction Method = Undefined | Production Ratio 40/39(k) = 0.000676 ± 0.000068 | |
| Heating = 60 sec | Production Ratio 38/39(k) = 0.012400 ± 0.003968 | |
| Isolation = 5.00 min | Production Ratio 36/38(cl) = 263.00 ± 13.15 | |
| Instrument = MAP-215-50 | Scaling Ratio K/Ca = 0.430 | |
| Lithology = Undefined | Abundance Ratio 40K/K = 1.1700 ± 0.0100 E-04 | |
| Lat-Lon = Undefined - Undefined | Atomic Weight K = 39.0983 ± 0.0001 g | |
| Feature = Undefined | | |

| Results | 40(a)/36(a) ± 2σ | 40(r)/39(k) ± 2σ | Age ± 2σ (Ma) | MSWD | 39Ar(k) (%,n) | K/Ca ± 2σ |
|---|---|---|---|---|---|---|
| **Age Plateau** | | 1.39862 ± 0.14998 | 1.67 ± 0.18 | 1.35 | 96.50 | 6 ± 9 |
| | | ± 10.72% | ± 10.72% | 20% | 11 | |
| Full External | | | ± 0.18 | 1.89 | 2σ Confidence Limit | |
| Analytical Error | | | ± 0.18 | 1.1615 | Error Magnification | |
| **Total Fusion** | | 1.39401 ± 0.19405 | 1.67 ± 0.23 | | 13 | 70 ± 170 |
| | | ± 13.92% | ± 13.92% | | | |
| Full External | | | ± 0.23 | | | |
| Analytical Error | | | ± 0.23 | | | |
| **Normal** | 301.58 ± 15.84 | 1.34360 ± 0.23522 | 1.61 ± 0.28 | 1.52 | 96.50 | |
| | ± 5.25% | ± 17.51% | ± 17.50% | 13% | 11 | |
| Full External | | | ± 0.28 | 1.94 | 2σ Confidence Limit | |
| Analytical Error | | | ± 0.28 | 1.2342 | Error Magnification | |
| | | | 11 | | Number of Iterations | |
| | | | ########## | | Convergence | |
| **Inverse** | 304.77 ± 15.64 | 1.32921 ± 0.22332 | 1.59 ± 0.27 | 1.40 | 96.50 | |
| | ± 5.13% | ± 16.80% | ± 16.80% | 18% | 11 | |
| Full External | | | ± 0.27 | 1.94 | 2σ Confidence Limit | |
| Analytical Error | | | ± 0.27 | 1.1822 | Error Magnification | |
| | | | 3 | | Number of Iterations | |
| | | | ########## | | Convergence | |
| | | | 37% | | Spreading Factor | |

## Supplementary Table 5 Duplicate Sample NZ1306 $^{39}Ar/^{40}Ar$ Analysis

| Relative Abundances | | | 36Ar [V] | %1σ | 37Ar [V] | %1σ | 38Ar [V] | %1σ | 39Ar [V] | %1σ | 40Ar [V] | %1σ | 40(r)/39(k) ± 2σ | Age ± 2σ (Ma) | 40Ar(r) (%) | 39Ar(k) (%) | K/Ca ± 2σ |
|---|---|---|---|---|---|---|---|---|---|---|---|---|---|---|---|---|---|
| 3M30284D | 64 °C | | 0.0000417 | 11.838 | 0.0001828 | 77.903 | 0.0000247 | 26.995 | 0.0013390 | 1.994 | 0.0166893 | 0.549 | 3.18437 ± 2.20792 | 3.80 ± 2.63 | 25.55 | 0.95 | 3.1 ± 4.9 |
| 3M30285D | 66 °C | | 0.0000752 | 7.427 | 0.0007866 | 20.402 | 0.0000580 | 11.492 | 0.0037047 | 1.489 | 0.0258456 | 0.475 | 0.92968 ± 0.90381 | 1.11 ± 1.08 | 13.32 | 2.63 | 2.0 ± 0.8 |
| 3M30286D | 67 °C | | 0.0000543 | 12.575 | 0.0002186 | 73.622 | 0.0000393 | 14.853 | 0.0025441 | 1.462 | 0.0165397 | 0.560 | 0.13804 ± 1.60381 | 0.16 ± 1.92 | 2.12 | 1.81 | 5.0 ± 7.4 |
| 3M30288D | 68 °C | 4 | 0.0005042 | 2.894 | 0.0000108 | 1528.223 | 0.0004260 | 2.463 | 0.0259352 | 0.463 | 0.1914379 | 0.212 | 1.57688 ± 0.33788 | 1.88 ± 0.40 | 21.36 | 18.44 | 1031.4 ± 31523.5 |
| 3M30289D | 69 °C | 4 | 0.0001399 | 4.798 | 0.0000620 | 260.955 | 0.0005977 | 2.427 | 0.0421606 | 0.408 | 0.0996201 | 0.158 | 1.37138 ± 0.09606 | 1.64 ± 0.11 | 58.04 | 29.98 | 292.3 ± 1525.7 |
| 3M30290D | 69 °C | 4 | 0.0000601 | 10.591 | 0.0001400 | 104.568 | 0.0001768 | 6.845 | 0.0127550 | 0.394 | 0.0329979 | 0.266 | 1.18145 ± 0.29828 | 1.41 ± 0.36 | 45.67 | 9.07 | 39.2 ± 81.9 |
| 3M30291D | 70 °C | 4 | 0.0001049 | 6.127 | 0.0000613 | 240.988 | 0.0001471 | 4.408 | 0.0093305 | 0.670 | 0.0418908 | 0.311 | 1.13353 ± 0.41257 | 1.35 ± 0.49 | 25.25 | 6.63 | 65.4 ± 315.4 |
| 3M30293D | 70 °C | 4 | 0.0000867 | 6.604 | 0.0000892 | 168.183 | 0.0000782 | 9.040 | 0.0044516 | 0.889 | 0.0307605 | 0.354 | 1.09762 ± 0.76975 | 1.31 ± 0.92 | 15.88 | 3.17 | 21.5 ± 72.2 |
| 3M30294D | 71 °C | 4 | 0.0000903 | 8.928 | 0.0000779 | 176.961 | 0.0000640 | 12.854 | 0.0040255 | 0.785 | 0.0308367 | 0.549 | 0.96216 ± 1.19941 | 1.15 ± 1.43 | 12.56 | 2.86 | 22.2 ± 78.7 |
| 3M30295D | 71 °C | 4 | 0.0000900 | 8.873 | 0.0000321 | 430.550 | 0.0000912 | 10.114 | 0.0055773 | 0.965 | 0.0306577 | 0.338 | 0.67861 ± 0.85602 | 0.81 ± 1.02 | 12.35 | 3.97 | 74.6 ± 642.7 |
| 3M30296D | 72 °C | 4 | 0.0000400 | 13.340 | 0.0001787 | 88.064 | 0.0000586 | 10.839 | 0.0047919 | 1.224 | 0.0198094 | 0.459 | 1.64519 ± 0.66702 | 1.97 ± 0.80 | 39.80 | 3.41 | 11.5 ± 20.3 |
| 3M30298D | 72 °C | 4 | 0.0000780 | 7.021 | 0.0002883 | 59.561 | 0.0001080 | 5.246 | 0.0066929 | 0.519 | 0.0296790 | 0.403 | 0.95995 ± 0.48983 | 1.15 ± 0.59 | 21.65 | 4.76 | 10.0 ± 11.9 |
| 3M30299D | 80 °C | 4 | 0.0000746 | 8.688 | 0.0002637 | 55.373 | 0.0001023 | 7.962 | 0.0068751 | 0.695 | 0.0320445 | 0.356 | 1.42413 ± 0.56426 | 1.70 ± 0.67 | 30.55 | 4.89 | 11.2 ± 12.4 |
| 3M30300D | 82 °C | 4 | 0.0001298 | 5.810 | 0.0001776 | 108.897 | 0.0001839 | 4.691 | 0.0104602 | 0.549 | 0.0537016 | 0.304 | 1.43138 ± 0.43182 | 1.71 ± 0.52 | 27.88 | 7.44 | 25.3 ± 55.2 |
| | | Σ | 0.0015695 | 1.757 | 0.0025481 | 22.962 | 0.0021558 | 1.501 | 0.1406436 | 0.190 | 0.6525108 | 0.092 | | | | | |

### Information on Analysis and Constants Used in Calculations

Sample = NZ1306C
Material = Msc
Location = Laser
Analyst = Fred Jourdan
Project = ALPINE SHIST_WH13
Mass Discrimination Law = POW
Irradiation = I17t3h
J = 0.00066100 ± 0.00000099
FCs = 28.294 ± 0.037 Ma
IGSN = Undefined
Preferred Age = Undefined
Classification = Undefined
Experiment Type = Undefined
Extraction Method = Undefined
Heating = 60 sec
Isolation = 5.00 min
Instrument = MAP-215-50
Lithology = Undefined
Lat-Lon = Undefined - Undefined
Feature = Undefined

Age Equations = Min et al. (2000)
Negative Intensities = Allowed
Decay Constant 40K = 5.531 ± 0.013 E-10 1/a
Decay Constant 39Ar = 2.940 ± 0.029 E-07 1/h
Decay Constant 37Ar = 8.230 ± 0.082 E-04 1/h
Decay Constant 36Cl = 2.303 ± 0.046 E-06 1/a
Decay Constant 40K(EC,$\beta^+$) = 0.576 ± 0.002 E-10 1/a
Decay Constant 40K($\beta^-$) = 4.955 ± 0.013 E-10 1/a
Atmospheric Ratio 40/36(a) = 298.56 ± 0.30
Atmospheric Ratio 38/36(a) = 0.1869 ± 0.0002
Production Ratio 39/37(ca) = 0.000706 ± 0.000049
Production Ratio 38/37(ca) = 0.000023 ± 0.000002
Production Ratio 36/37(ca) = 0.000281 ± 0.000008
Production Ratio 40/39(k) = 0.000676 ± 0.000068
Production Ratio 38/39(k) = 0.012400 ± 0.003968
Production Ratio 36/38(cl) = 263.00 ± 13.15
Scaling Ratio K/Ca = 0.430
Abundance Ratio 40K/K = 1.1700 ± 0.0100 E-04
Atomic Weight K = 39.0983 ± 0.0001 g

| Results | 40(a)/36(a) ± 2σ | 40(r)/39(k) ± 2σ | Age ± 2σ (Ma) | MSWD | 39Ar(k) (%,n) | K/Ca ± 2σ |
|---|---|---|---|---|---|---|
| **Age Plateau** | | 1.34498 ± 0.08560 (± 6.36%) | 1.61 ± 0.10 (± 6.37%) | 1.12 | 94.61 | 11.5 ± 7.7 |
| | | Full External Error ± 0.10 | | 34% | 11 | |
| | | Analytical Error ± 0.10 | | 1.89 | 2σ Confidence Limit | |
| | | | | 1.0585 | Error Magnification | |
| **Total Fusion Age** | | 1.30853 ± 0.11754 (± 8.98%) | 1.56 ± 0.14 (± 8.98%) | | 14 | 23.7 ± 10.9 |
| | | Full External Error ± 0.14 | | | | |
| | | Analytical Error ± 0.14 | | | | |
| **Normal Isochron** | 295.85 ± 19.72 (± 6.67%) | 1.34104 ± 0.15137 (± 11.29%) | 1.60 ± 0.18 (± 11.29%) | 1.40 | 94.61 | |
| | | Full External Error ± 0.18 | | 18% | 11 | |
| | | Analytical Error ± 0.18 | | 1.94 | 2σ Confidence Limit | |
| | | | | 1.1824 | Error Magnification | |
| | | | | 23 | Number of Iterations | |
| | | | | 0.0000125280 | Convergence | |
| **Inverse Isochron** | 299.23 ± 18.68 (± 6.24%) | 1.34124 ± 0.13755 (± 10.26%) | 1.60 ± 0.16 (± 10.26%) | 1.24 | 94.61 | |
| | | Full External Error ± 0.16 | | 26% | 11 | |
| | | Analytical Error ± 0.16 | | 1.94 | 2σ Confidence Limit | |
| | | | | 1.1154 | Error Magnification | |
| | | | | 3 | Number of Iterations | |
| | | | | 0.0002809484 | Convergence | |
| | | | | 39% | Spreading Factor | |

## Supplementary Table 6 Sample NZ1309 $^{39}Ar/^{40}Ar$ Analysis

| Relative Abundances | | | 36Ar [V] | %1σ | 37Ar [V] | %1σ | 38Ar [V] | %1σ | 39Ar [V] | %1σ | 40Ar [V] | %1σ | 40(r)/39(k) ± 2σ | Age ± 2σ (Ma) | 40Ar(r) (%) | 39Ar(k) (%) | K/Ca ± 2σ |
|---|---|---|---|---|---|---|---|---|---|---|---|---|---|---|---|---|---|
| 3M30336D | 66 °C | 4 | 0.0000589 | 8.156 | 0.0001630 | 101.486 | 0.0000222 | 29.548 | 0.0003668 | 3.183 | 0.0174509 | 0.541 | 0.38079 ± 7.83269 | 0.46 ± 9.36 | 0.80 | 1.68 | 1.0 ± 2.0 |
| 3M30338D | 68 °C | 4 | 0.0000973 | 8.187 | 0.0001458 | 122.896 | 0.0000479 | 14.552 | 0.0020094 | 0.717 | 0.0327879 | 0.376 | 1.84941 ± 2.37139 | 2.21 ± 2.83 | 11.33 | 9.23 | 5.9 ± 14.6 |
| 3M30339D | 69 °C | 4 | 0.0000991 | 5.485 | 0.0000654 | 279.592 | 0.0001358 | 5.906 | 0.0079827 | 1.077 | 0.0450327 | 0.265 | 1.93500 ± 0.40978 | 2.31 ± 0.49 | 34.30 | 36.66 | 52.4 ± 293.3 |
| 3M30340D | 69 °C | 4 | 0.0000791 | 6.824 | 0.0000696 | 238.503 | 0.0000544 | 16.520 | 0.0027933 | 1.176 | 0.0295945 | 0.314 | 2.13922 ± 1.15682 | 2.55 ± 1.38 | 20.19 | 12.83 | 17.3 ± 82.3 |
| 3M30341D | 70 °C | 4 | 0.0001313 | 6.668 | 0.0000131 | 1224.740 | 0.0000353 | 17.586 | 0.0010984 | 1.862 | 0.0388490 | 0.190 | 0.31625 ± 4.76082 | 0.38 ± 5.69 | 0.89 | 5.04 | 36.1 ± 884.3 |
| 3M30343D | 70 °C | 4 | 0.0000571 | 11.287 | 0.0000503 | 338.118 | 0.0000212 | 30.368 | 0.0005040 | 2.326 | 0.0195019 | 0.391 | 4.84005 ± 7.64932 | 5.78 ± 9.11 | 12.51 | 2.31 | 4.3 ± 29.1 |
| 3M30344D | 71 °C | 4 | 0.0000787 | 7.994 | 0.0000551 | 290.466 | 0.0000269 | 22.727 | 0.0006272 | 2.478 | 0.0235110 | 0.378 | 0.04975 ± 5.99400 | 0.06 ± 7.16 | 0.13 | 2.88 | 4.9 ± 28.4 |
| 3M30345D | 71 °C | 4 | 0.0001089 | 4.887 | 0.0000043 | 4128.749 | 0.0000322 | 19.173 | 0.0010478 | 2.324 | 0.0337650 | 0.472 | 1.19363 ± 3.04916 | 1.43 ± 3.64 | 3.70 | 4.81 | 105.4 ± 8707.5 |
| 3M30346D | 72 °C | 4 | 0.0000508 | 12.397 | 0.0000779 | 220.648 | 0.0000159 | 36.513 | 0.0005443 | 2.493 | 0.0163626 | 0.446 | 2.22348 ± 6.91235 | 2.66 ± 8.25 | 7.40 | 2.50 | 3.0 ± 13.3 |
| 3M30348D | 72 °C | 4 | 0.0000917 | 5.024 | 0.0000457 | 368.871 | 0.0000380 | 14.806 | 0.0009216 | 3.308 | 0.0283202 | 0.296 | 1.01918 ± 2.99210 | 1.22 ± 3.57 | 3.32 | 4.23 | 8.7 ± 63.9 |
| 3M30349D | 80 °C | 4 | 0.0000915 | 7.947 | 0.0000550 | 321.665 | 0.0000384 | 20.195 | 0.0015956 | 1.088 | 0.0282666 | 0.323 | 0.58641 ± 2.72438 | 0.70 ± 3.25 | 3.31 | 7.33 | 12.5 ± 80.3 |
| 3M30350D | 82 °C | 4 | 0.0001547 | 4.598 | 0.0000306 | 573.350 | 0.0000521 | 14.165 | 0.0022835 | 1.511 | 0.0501557 | 0.200 | 1.73969 ± 1.86298 | 2.08 ± 2.22 | 7.92 | 10.49 | 32.1 ± 367.8 |
| | | Σ | 0.0010990 | 2.026 | 0.0005013 | 118.357 | 0.0005205 | 4.598 | 0.0217746 | 0.520 | 0.3635981 | 0.096 | | | | | |

### Information on Analysis and Constants Used in Calculations

Sample = NZ1309B
Material = Msc
Location = Laser
Analyst = Fred Jourdan
Project = ALPINE SHIST_WH13
Mass Discrimination Law = POW
Irradiation = I17t3h
J = 0.00066100 ± 0.00000100
FCs = 28.294 ± 0.037 Ma
IGSN = Undefined
Preferred Age = Undefined
Classification = Undefined
Experiment Type = Undefined
Extraction Method = Undefined
Heating = 60 sec
Isolation = 5.00 min
Instrument = MAP-215-50
Lithology = Undefined
Lat-Lon = Undefined - Undefined
Feature = Undefined

Age Equations = Min et al. (2000)
Negative Intensities = Allowed
Decay Constant 40K = 5.531 ± 0.013 E-10 1/a
Decay Constant 39Ar = 2.940 ± 0.029 E-07 1/h
Decay Constant 37Ar = 8.230 ± 0.082 E-04 1/h
Decay Constant 36Cl = 2.303 ± 0.046 E-06 1/a
Decay Constant 40K(EC,$\beta^+$) = 0.576 ± 0.002 E-10 1/a
Decay Constant 40K($\beta^-$) = 4.955 ± 0.013 E-10 1/a
Atmospheric Ratio 40/36(a) = 298.56 ± 0.30
Atmospheric Ratio 38/36(a) = 0.1869 ± 0.0002
Production Ratio 39/37(ca) = 0.000706 ± 0.000049
Production Ratio 38/37(ca) = 0.000023 ± 0.000002
Production Ratio 36/37(ca) = 0.000281 ± 0.000008
Production Ratio 40/39(k) = 0.000676 ± 0.000068
Production Ratio 38/39(k) = 0.012400 ± 0.003968
Production Ratio 36/38(cl) = 263.00 ± 13.15
Scaling Ratio K/Ca = 0.430
Abundance Ratio 40K/K = 1.1700 ± 0.0100 E-04
Atomic Weight K = 39.0983 ± 0.0001 g

| Results | 40(a)/36(a) ± 2σ | 40(r)/39(k) ± 2σ | Age ± 2σ (Ma) | MSWD | 39Ar(k) (%,n) | K/Ca ± 2σ |
|---|---|---|---|---|---|---|
| **Age Plateau** | | 1.88055 ± 0.36158 ± 19.23% | 2.25 ± 0.43 ± 19.22% | 0.35 | 100.00 | 1.0 ± 1.9 |
| | | | Full External Error ± 0.43 | 97% | 12 | |
| | | | Analytical Error ± 0.43 | 1.85 | 2σ Confidence Limit | |
| | | | | 1.0000 | Error Magnification | |
| **Total Fusion Age** | | 1.62713 ± 0.61163 ± 37.59% | 1.94 ± 0.73 ± 37.57% | | 12 | 18.7 ± 44.2 |
| | | | Full External Error ± 0.73 | | | |
| | | | Analytical Error ± 0.73 | | | |
| **Normal Isochron** | 288.83 ± 14.99 ± 5.19% | 2.08297 ± 0.47941 ± 23.02% | 2.49 ± 0.57 ± 23.00% | 0.25 | 100.00 | |
| **Overestimated Error** | | | Full External Error ± 0.57 | 99% | 12 | |
| | | | Analytical Error ± 0.57 | 1.89 | 2σ Confidence Limit | |
| | | | | 1.0000 | Error Magnification | |
| | | | | 9 | Number of Iterations | |
| | | | | 0.0000129654 | Convergence | |
| **Inverse Isochron** | 289.85 ± 15.10 ± 5.21% | 2.07259 ± 0.47280 ± 22.81% | 2.48 ± 0.56 ± 22.80% | 0.26 | 100.00 | |
| **Overestimated Error** | | | Full External Error ± 0.56 | 99% | 12 | |
| | | | Analytical Error ± 0.56 | 1.89 | 2σ Confidence Limit | |
| | | | | 1.0000 | Error Magnification | |
| | | | | 3 | Number of Iterations | |
| | | | | 0.0000019206 | Convergence | |
| | | | | 32% | Spreading Factor | |

## Supplementary Table 7 Sample NZ1312 $^{39}Ar/^{40}Ar$ Analysis

| Relative Abundances | | | 36Ar [V] | %1σ | 37Ar [V] | %1σ | 38Ar [V] | %1σ | 39Ar [V] | %1σ | 40Ar [V] | %1σ | 40(r)/39(k) ± 2σ | Age ± 2σ (Ma) | 40Ar(r) (%) | 39Ar(k) (%) | K/Ca ± 2σ |
|---|---|---|---|---|---|---|---|---|---|---|---|---|---|---|---|---|---|
| 3M30258D | 69 °C | 4 | 0.0001187 | 9.974 | 0.0001553 | 185.487 | 0.0000408 | 13.563 | 0.0020970 | 1.783 | 0.0356675 | 0.386 | 0.11071 ± 3.37503 | 0.13 ± 4.03 | 0.65 | 11.29 | 5.8 ± 21.5 |
| 3M30259D | 69 °C | 4 | 0.0000957 | 10.675 | 0.0000689 | 435.239 | 0.0001538 | 7.169 | 0.0112650 | 0.690 | 0.0470926 | 0.295 | 1.64315 ± 0.54275 | 1.96 ± 0.65 | 39.31 | 60.65 | 70.3 ± 611.8 |
| 3M30261D | 72 °C | 4 | 0.0001516 | 7.489 | 0.0001259 | 226.327 | 0.0000433 | 13.233 | 0.0009459 | 1.982 | 0.0469543 | 0.371 | 1.79072 ± 7.17938 | 2.14 ± 8.57 | 3.61 | 5.09 | 3.2 ± 14.6 |
| 3M30263D | 80 °C | 4 | 0.0001014 | 8.663 | 0.0000134 | 2141.534 | 0.0000347 | 15.397 | 0.0010949 | 2.325 | 0.0358748 | 0.384 | 5.10834 ± 4.80517 | 6.10 ± 5.72 | 15.59 | 5.89 | 35.1 ± 1503.4 |
| 3M30264D | 82 °C | 4 | 0.0000958 | 10.543 | 0.0000666 | 439.922 | 0.0000569 | 12.222 | 0.0031723 | 0.823 | 0.0397125 | 0.326 | 3.49993 ± 1.90387 | 4.18 ± 2.27 | 27.96 | 17.08 | 20.5 ± 180.3 |
| | | Σ | 0.0005633 | 4.174 | 0.0002969 | 218.873 | 0.0003294 | 4.912 | 0.0185752 | 0.514 | 0.2053017 | 0.157 | | | | | |

**Information on Analysis and Constants Used in Calculations**

Sample = NZ1312B
Material = Msc
Location = Laser
Analyst = Fred Jourdan
Project = ALPINE SHIST_WH13
Mass Discrimination Law = POW
Irradiation = I17t3h
J = 0.00066100 ± 0.00000099
FCs = 28.294 ± 0.037 Ma
IGSN = Undefined
Preferred Age = Undefined
Classification = Undefined
Experiment Type = Undefined
Extraction Method = Undefined
Heating = 60 sec
Isolation = 5.00 min
Instrument = MAP-215-50
Lithology = Undefined
Lat-Lon = Undefined - Undefined
Feature = Undefined

Age Equations = Min et al. (2000)
Negative Intensities = Allowed
Decay Constant 40K = 5.531 ± 0.013 E-10 1/a
Decay Constant 39Ar = 2.940 ± 0.029 E-07 1/h
Decay Constant 37Ar = 8.230 ± 0.082 E-04 1/h
Decay Constant 36Cl = 2.303 ± 0.046 E-06 1/a
Decay Constant 40K(EC,$\beta^+$) = 0.576 ± 0.002 E-10 1/a
Decay Constant 40K($\beta^-$) = 4.955 ± 0.013 E-10 1/a
Atmospheric Ratio 40/36(a) = 298.56 ± 0.30
Atmospheric Ratio 38/36(a) = 0.1869 ± 0.0002
Production Ratio 39/37(ca) = 0.000706 ± 0.000049
Production Ratio 38/37(ca) = 0.000023 ± 0.000002
Production Ratio 36/37(ca) = 0.000281 ± 0.000008
Production Ratio 40/39(k) = 0.000676 ± 0.000068
Production Ratio 38/39(k) = 0.012400 ± 0.003968
Production Ratio 36/38(cl) = 263.00 ± 13.15
Scaling Ratio K/Ca = 0.430
Abundance Ratio 40K/K = 1.1700 ± 0.0100 E-04
Atomic Weight K = 39.0983 ± 0.0001 g

| Results | 40(a)/36(a) ± 2σ | 40(r)/39(k) ± 2σ | Age ± 2σ (Ma) | MSWD | 39Ar(k) (%,n) | K/Ca ± 2σ |
|---|---|---|---|---|---|---|
| **Age Plateau** | | 1.78203 ± 0.64791 ± 36.36% | 2.13 ± 0.77 ± 36.34% | 1.60 | 100.00 | 4.0 ± 12.1 |
| | | | | 17% | 5 | |
| | | | Full External Error ± 0.77 | 2.41 | 2σ Confidence Limit | |
| | | | Analytical Error ± 0.77 | 1.2665 | Error Magnification | |
| **Total Fusion Age** | | 1.99904 ± 0.75698 ± 37.87% | 2.39 ± 0.90 ± 37.84% | | 5 | 26.9 ± 117.7 |
| | | | Full External Error ± 0.90 | | | |
| | | | Analytical Error ± 0.90 | | | |
| **Normal Isochron** | 308.98 ± 40.91 ± 13.24% | 1.57466 ± 0.84668 ± 53.77% | 1.88 ± 1.01 ± 53.74% | 1.60 | 100.00 | |
| | | | | 19% | 5 | |
| | | | Full External Error ± 1.01 | 2.63 | 2σ Confidence Limit | |
| | | | Analytical Error ± 1.01 | 1.2636 | Error Magnification | |
| | | | | 9 | Number of Iterations | |
| | | | | 0.0000108491 | Convergence | |
| **Inverse Isochron** | 318.08 ± 43.06 ± 13.54% | 1.53058 ± 0.77225 ± 50.45% | 1.83 ± 0.92 ± 50.43% | 1.63 | 100.00 | |
| | | | | 18% | 5 | |
| | | | Full External Error ± 0.92 | 2.63 | 2σ Confidence Limit | |
| | | | Analytical Error ± 0.92 | 1.2781 | Error Magnification | |
| | | | | 3 | Number of Iterations | |
| | | | | 0.0000000261 | Convergence | |
| | | | | 34% | Spreading Factor | |

## Supplementary Table 8 Duplicate Sample NZ1312 $^{39}Ar/^{40}Ar$ Analysis

| Relative Abundances | | | 36Ar [V] | %1σ | 37Ar [V] | %1σ | 38Ar [V] | %1σ | 39Ar [V] | %1σ | 40Ar [V] | %1σ | 40(r)/39(k) ± 2σ | Age ± 2σ (Ma) | 40Ar(r) (%) | 39Ar(k) (%) | K/Ca ± 2σ |
|---|---|---|---|---|---|---|---|---|---|---|---|---|---|---|---|---|---|
| 3M30302D | 64 °C | 4 | 0.0000575 | 11.235 | 0.0031965 | 5.986 | 0.0000239 | 20.404 | 0.0006493 | 2.256 | 0.0194899 | 0.562 | 4.00611 ± 5.97347 | 4.78 ± 7.12 | 13.30 | 1.06 | 0.09 ± 0.01 |
| 3M30303D | 66 °C | 4 | 0.0000925 | 7.538 | 0.0072225 | 3.638 | 0.0000364 | 18.684 | 0.0015573 | 1.244 | 0.0304044 | 0.328 | 2.18760 ± 2.68625 | 2.61 ± 3.21 | 11.17 | 2.54 | 0.09 ± 0.01 |
| 3M30304D | 67 °C | 4 | 0.0000487 | 13.580 | 0.0040318 | 6.163 | 0.0000273 | 18.882 | 0.0013274 | 1.556 | 0.0175533 | 0.760 | 2.52270 ± 2.99132 | 3.01 ± 3.57 | 19.04 | 2.17 | 0.14 ± 0.02 |
| 3M30306D | 68 °C | 4 | 0.0003143 | 2.822 | 0.0016662 | 10.832 | 0.0002042 | 3.422 | 0.0124528 | 0.681 | 0.1167756 | 0.174 | 1.85332 ± 0.42758 | 2.21 ± 0.51 | 19.76 | 20.40 | 3.21 ± 0.70 |
| 3M30307D | 69 °C | 4 | 0.0001590 | 4.399 | 0.0002321 | 67.592 | 0.0004129 | 4.007 | 0.0294949 | 0.556 | 0.0989219 | 0.170 | 1.74405 ± 0.14346 | 2.08 ± 0.17 | 52.00 | 48.33 | 54.64 ± 73.87 |
| 3M30308D | 69 °C | 4 | 0.0000950 | 7.939 | 0.0002768 | 64.092 | 0.0001559 | 5.807 | 0.0116867 | 0.530 | 0.0501721 | 0.255 | 1.86704 ± 0.38661 | 2.23 ± 0.46 | 43.49 | 19.15 | 18.16 ± 23.27 |
| 3M30309D | 70 °C | 4 | 0.0000679 | 9.451 | 0.0004623 | 26.863 | 0.0000650 | 7.974 | 0.0038742 | 1.108 | 0.0258461 | 0.414 | 1.44859 ± 0.99120 | 1.73 ± 1.18 | 21.71 | 6.35 | 3.60 ± 1.94 |
| | | Σ | 0.0008349 | 2.272 | 0.0170883 | 3.049 | 0.0009257 | 2.482 | 0.0610427 | 0.331 | 0.3591634 | 0.103 | | | | | |

## Information on Analysis and Constants Used in Calculations

Sample = NZ1312C
Material = Msc
Location = Laser
Analyst = Fred Jourdan
Project = ALPINE SHIST_WH13
Mass Discrimination Law = POW
Irradiation = I17t3h
J = 0.00066100 ± 0.00000100
FCs = 28.294 ± 0.037 Ma
IGSN = Undefined
Preferred Age = Undefined
Classification = Undefined
Experiment Type = Undefined
Extraction Method = Undefined
Heating = 60 sec
Isolation = 5.00 min
Instrument = MAP-215-50
Lithology = Undefined
Lat-Lon = Undefined - Undefined
Feature = Undefined

Age Equations = Min et al. (2000)
Negative Intensities = Allowed
Decay Constant 40K = 5.531 ± 0.013 E-10 1/a
Decay Constant 39Ar = 2.940 ± 0.029 E-07 1/h
Decay Constant 37Ar = 8.230 ± 0.082 E-04 1/h
Decay Constant 36Cl = 2.303 ± 0.046 E-06 1/a
Decay Constant 40K(EC,β⁺) = 0.576 ± 0.002 E-10 1/a
Decay Constant 40K(β⁻) = 4.955 ± 0.013 E-10 1/a
Atmospheric Ratio 40/36(a) = 298.56 ± 0.30
Atmospheric Ratio 38/36(a) = 0.1869 ± 0.0002
Production Ratio 39/37(ca) = 0.000706 ± 0.000049
Production Ratio 38/37(ca) = 0.000023 ± 0.000002
Production Ratio 36/37(ca) = 0.000281 ± 0.000008
Production Ratio 40/39(k) = 0.000676 ± 0.000068
Production Ratio 38/39(k) = 0.012400 ± 0.003968
Production Ratio 36/38(cl) = 263.00 ± 13.15
Scaling Ratio K/Ca = 0.430
Abundance Ratio 40K/K = 1.1700 ± 0.0100 E-04
Atomic Weight K = 39.0983 ± 0.0001 g

| Results | 40(a)/36(a) ± 2σ | 40(r)/39(k) ± 2σ | Age ± 2σ (Ma) | MSWD | 39Ar(k) (%,n) | K/Ca ± 2σ |
|---|---|---|---|---|---|---|
| **Age Plateau** | | 1.76551 ± 0.12695 ± 7.19% | 2.11 ± 0.15 ± 7.19% | 0.31 | 100.00 | 0.10 ± 0.03 |
| | | | | 93% | 7 | |
| | | Full External Error ± 0.15 | | 2.15 | 2σ Confidence Limit | |
| | | Analytical Error ± 0.15 | | 1.0000 | Error Magnification | |
| **Total Fusion Age** | | 1.82330 ± 0.18642 ± 10.22% | 2.18 ± 0.22 ± 10.22% | | 7 | 1.54 ± 0.09 |
| | | Full External Error ± 0.22 | | | | |
| | | Analytical Error ± 0.22 | | | | |
| **Normal Isochron** | 305.18 ± 19.85 ± 6.50% | 1.71052 ± 0.20293 ± 11.86% | 2.04 ± 0.24 ± 11.86% | 0.26 | 100.00 | |
| **Overestimated Error** | | | | 93% | 7 | |
| | | Full External Error ± 0.24 | | 2.26 | 2σ Confidence Limit | |
| | | Analytical Error ± 0.24 | | 1.0000 | Error Magnification | |
| | | | | 15 | Number of Iterations | |
| | | | | 0.0000122425 | Convergence | |
| **Inverse Isochron** | 305.87 ± 19.88 ± 6.50% | 1.70820 ± 0.20197 ± 11.82% | 2.04 ± 0.24 ± 11.82% | 0.26 | 100.00 | |
| **Overestimated Error** | | | | 94% | 7 | |
| | | Full External Error ± 0.24 | | 2.26 | 2σ Confidence Limit | |
| | | Analytical Error ± 0.24 | | 1.0000 | Error Magnification | |
| | | | | 3 | Number of Iterations | |
| | | | | 0.0000044974 | Convergence | |
| | | | | 45% | Spreading Factor | |

Appendix Extended $^{40}Ar/^{39}Ar$ Dating Method

We selected 3 fresh samples from the mylonite zone of the Alpine Schist for $^{40}Ar/^{39}Ar$ dating, he location of each sample is given in Supplementary Table 9.

**Supplementary Table 9 Latitude and Longitude Coordinates of Muscovite Samples**

| Sample | GPS |
|---|---|
| NZ1306 | $43^0$ 23' 15.9" S $170^0$ 12'15.1" E |
| NZ1309 | $43^0$ 23' 16.5" S $170^0$ 12'18.8" E |
| NZ1312 | $43^0$ 23' 17.7" S $170^0$ 12'32.5" E |

The samples were initially cut down to a size appropriate for the Jaw Crusher using a Latham Allegro Supercut Saw located in the basement of the Mawson Building at the University of Adelaide. When setting up ensure that the stage of the saw is running free and examine the blade for visible damage. To avoid contamination from previous samples clean the surface of the stage and blade with water. Once cleaned place the hand sample on the stage and ensure that the size and orientation of the sample will not result in it making contact with the arbor or the shaft of the saw as it is cut. If the sample is unstable washed brick blocks may be positioned to stabilise the sample. Turn on the water directed onto the blade, adjust so that there is minor splashback and adequate blade wetting for quality and safe cutting. Firmly grip the sample on the stage and gently push the sample into the blade. As you approach the end of the cut slow down the feed rate so that the blade just cuts off the desired section. The desired size for crushing is no greater than 10 cm in any dimension. Cut samples are dried on hot plates ready for crushing.

The initial crushing was performed by the large jaw crusher in the basement of the Mawson Building, The University of Adelaide. To avoid contamination open the jaw crusher and clean the jaw crusher jaws with a wire brush ensuring no fragments are caught in the equipment. Then clean the jaw crusher and collection tray with compressed air and then ethanol and paper towel. Dry the equipment with compressed air. Line the collection tray with A3 sheets of paper. Close the jaw crusher and replace the collection tray. Turn on the jaw crusher and drop samples through the sample chute into the moving jaws and close the sample chute lid to prevent sample loss.

Crushed samples are then milled using the Pulverisette 13 Disc Mill in the basement of the Mawson Building, The University of Adelaide. To avoid contamination the disc mill should be cleaned. Open the cover and clean the mill and collection hopper with compressed air and then paper towel and ethanol. Dry the equipment with compressed air and reassemble. Set the gap between the discs with the screw adjustment wheel and locking nut handle at the end of the grinder. Initially adjust gap to 5 mm. Put the sample through the first pass then collect the sample from the hopper and reprocess at disc gaps of 3 mm, 1 mm and final pass of 0.5 mm. The sample is then ready to be separated by sieving.

The sieve setup requires an EFL 2000 shaker, Flexistack with a base, 2 rings and a lid. Nylon mesh is required for the rings at 400 µm and 79 µm mesh size. Initially all flexistack components should be cleaned using paper towel and ethanol then dried with compressed air. The flexistack is prepared with the 400 µm mesh in the top ring and 79 µm mesh in the bottom ring. Assemble the stack with the base for collecting fines, bottom ring, top ring and then place sample on 400 µm mesh of the top ring. Place the lid on top of the top ring. A schematic diagram of the sieve setup is seen in Supplementary Figure 1. The flexistack should then be placed into the EFL 2000. The flexistack is locked in place with the nuts and levers. The EFL 2000 should be turned on for 1 minute to allow for sufficient time to separate

the sample into the size fractions. Turn off the EFL 2000 and remove the flexistack. The coarse fraction > 400 µm should be placed in a labelled sample bag. Subsequently the middle section between 400 µm and 79 µm should be removed and placed in a separate labelled sample bag for further processing. The fine fraction < 79 µm should be removed from the bottom and placed in a separate labelled sample bag. The nylon mesh should be removed from the top and bottom rings and placed in a separate labelled sample bag.

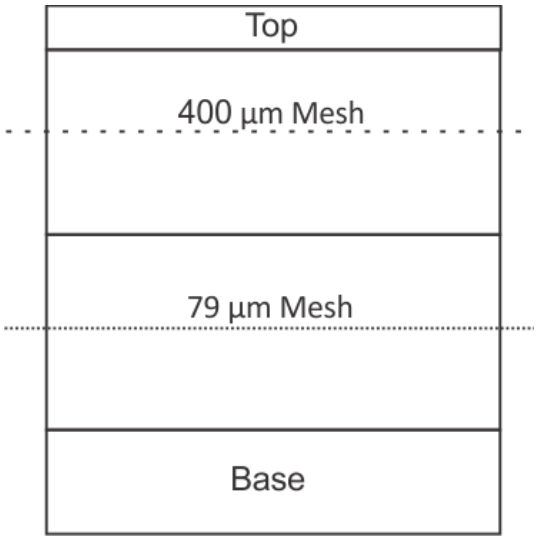


**Supplementary Figure 1 Schematic sieve setup diagram**

Magnetic separation of the middle fraction between 400 µm and 79 µm was performed using a Frantz Isodynamic Separator Model L-1. The Frantz was initially cleaned to remove sample contaminants. Initially remove the inclined chute by unscrewing from the Frantz. Clean the chute, collection tins, sample funnel and Frantz using compressed air. Ensure that no residual paramagnetic material remains on the electromagnet. Position and screw the chute back into position. The inclined chute of the Frantz was set to an angle of 15 degrees. The amperes setting for the magnet was set at 1.2 amps. The coaxial vibrator was set to 10 on the 10 turn potentiometer. The coaxial vibrator and electromagnet are switched on.
The sample fraction between 79 and 400 µm was poured in lines on a clean sheet of A4 paper and then magnetic minerals were removed by running a hand magnet over the sample minerals. Any magnetic component was removed and discarded.

The sample fraction was poured into the sample funnel at the top of the separator ramp. The more strongly paramagnetic minerals are separated on the high side of the dividing edge with the more weakly muscovite containing fraction in the lower side. Both fractions divided are collected and placed in separate labelled bags.
To create a pure muscovite sample the weakly magnetic separate was handpicked under an Olympus SZ61 optical binocular microscope. Hand picking involved the selection of pure, unaltered, optically transparent muscovite grains. To avoid recoil problems in later stage irradiation, no grains <130 µm in diameter were picked. The final sample weight of muscovite was > 50 mg.
For Ar/Ar dating the Muscovite grains were leached in dilute HF for 1 minute then rinsed with distilled water in an ultrasonic cleaner. The samples were loaded into large wells of diameter 19 mm with aluminium discs of 3mm depth. Each well was bracketed by smaller wells that included Fish Canyon sanidine used as a neutron fluence monitor. The age of the

Fish Canyon sanidine has an adopted age of 28.305 ± 0.036 Ma (1σ) from work done by Renne et al. (2010) based on the calibration work of Jourdan and Renne (2007). The sample discs were Cd-shielded and irradiated in the Hamilton McMaster University nuclear reactor (Canada) in position 5C. The mean J-values computed from the standard grains within the small pits range from $0.00066100 \pm 0.99\times10^{-6}$ (0.15%) to $0.0066100 \pm 1.0\times10^{-6}$ (0.16%). These were used to determine the average and standard deviation of J-values of each irradiation disc.Mass discrimination was monitored using an automated air pipette and provided a mean value of 1.006286 ± 0.00342 per Dalton (Da), relative to an air ratio of 298.56 ± 0.31 from the calculations of Lee et al. (2006). The correction factors for interfering isotopes are seen in Suuplementary Table 10.

**Supplementary Table 10 Interfering Isotopes Correction Factors**

| Interfering Isotope System | Correction Factor |
|---|---|
| $(^{39}Ar/^{37}Ar)_{Ca}$ | 7.30x10-4 (±11%) |
| $(^{36}Ar/^{37}Ar)_{Ca}$ | 2.82x10-4 (± 1%) |
| $(^{40}Ar/^{39}Ar)_{K}$ | 6.76x10-4 (± 32%) |

The $^{40}Ar/^{39}Ar$ analyses were performed at the Western Australian Argon Isotope Facility (WAAIF) at Curtin University, operated by a consortium consisting of Curtin University and the University of Western Australia. The samples were step-heated using a 110 W Spectron Laser System with a continuous Nd-YAG (IR; 1064 nm) laser rastered over the sample during 1 minute to ensure a homogenously distributed temperature. To purify the gas a stainless steel extraction line using three SAES AP10 getters and a liquid nitrogen condensation trap was linked to the system.
To measure Ar isotopes in static mode a MAP 215-50 mass spectrometer (resolution of ~500; sensitivity of $4x10^{-14}$ mol/V) was used with a Balzers SEV 217 electron multiplier using 10 cycles of peak-hopping. Data acquisition was performed using the Argus program written by M.O. McWilliams and ran under a LabView environment. Raw data processing used ArArCALC software (Koppers 2002) with ages calculated using the decay constants recommended from the work of Renne et al. (2010).

To calculate plateau ages [Figure 11 and Table 9] at the 2σ level the mean of all plateau steps was used, each plateau step is weighted by the inverse variance of the respective analytical error. Plateau criteria requires, at least 70% of $^{39}Ar$, distributed over a minimum of 3 consecutive steps with agreement at the 95% confidence interval and satisfying a p value (probability of fit) of at least 0.05. Mini plateaus criteria are defined by the same as for plateaus except include between 50% and 70% $^{39}Ar$.

The calculation of integrated ages (2σ) uses the total gas released for each Ar isotope. The inverse isochrones include the maximum number of steps with a p value of $\geq 0.05$. All sources of uncertainties are included in the calculation.

Zircon Dating
A total of 6 rock samples from the Alpine Schist were selected from the locations in Supplementary Table 11, for U/Pb dating of zircons.

**Supplementary Table 11 Rock Sample GPS Locations**

| Sample | GPS Coordinates |
|---|---|
| NZ1309 | 43° 23' 15.9" S 170° 12'15.1" E |
| NZ1310 | 43° 23' 17.7" S 170° 12'32.5" E |
| NZ1315 | 43° 23' 15.9" S 170° 12'15.1" E |

The samples were initially cut down to a size appropriate for the Jaw Crusher using a Latham Allegro Supercut Saw located in the basement of the Mawson Building at the University of Adelaide. When setting up the saw ensure that the stage is running free and examine the blade for visible damage. To avoid contamination from previous samples clean the surface of the stage and blade with water. Once cleaned place the hand sample on the stage and ensure that the size and orientation of the sample will not result in it making contact with the arbor or the shaft of the saw as it is cut. If the sample is unstable washed brick blocks may be positioned to stabilise the sample. Turn on the water jets directed onto the blade, adjust so that there is minor splashback and adequate blade wetting for quality and safe cutting. Firmly grip the sample on the stage and gently push the sample into the blade. As you approach the end of the cut slow down the feed rate so that the blade just cuts off the desired section. The desired size for crushing is no greater than 10 cm in any dimension. Cut samples are dried on hot plates ready for crushing.

The initial crushing was performed by the large jaw crusher in the basement of the Mawson Building, The University of Adelaide. To avoid contamination open the jaw crusher and clean the jaw crusher jaws with a wire brush ensuring no fragments are caught in the equipment. Then clean the jaw crusher and collection tray with compressed air and then ethanol and paper towel. Dry the equipment with compressed air. Line the collection tray with A3 sheets of paper. Close the jaw crusher and replace the collection tray. Turn on the jaw crusher and drop samples through the sample chute into the moving jaws and close the sample chute lid to prevent sample loss.

Crushed samples are then milled using the Pulverisette 13 Disc Mill in the basement of the Mawson Building, The University of Adelaide. To avoid contamination the disc mill should be cleaned. Open the cover and clean the mill and collection hopper with compressed air and then paper towel and ethanol. Dry the equipment with compressed air and reassemble. Set the gap between the discs with the screw adjustment wheel and locking nut handle at the end of the grinder. Initially adjust gap to 5 mm. Put the sample through the first pass then collect the sample from the hopper and reprocess at disc gaps of 3 mm, 1 mm and final pass of 0.5 mm. The sample is then ready to be separated by sieving.

The sieve setup requires an EFL 2000 shaker, Flexistack with a base, 2 rings and a lid. Nylon mesh is required for the rings at 400 µm and 79 µm mesh size. Initially all flexistack components should be cleaned using paper towel and ethanol then dried with compressed air. The flexistack is prepared with the 400 µm mesh in the top ring and 79 µm mesh in the bottom ring. Assemble the stack with the base for collecting fines, bottom ring, top ring and then place sample on 400 µm mesh of the top ring. Place the lid on top of the top ring. Sample should then be placed into the EFL 2000. The flexistack is locked in place with the nuts and levers. The EFL 2000 should be turned on for 1 minute to allow for sufficient time to separate the sample into the size fractions. Turn off the EFL 2000 and remove the flexistack. The coarse fraction > 400 µm should be placed in a labelled sample bag. Subsequently the middle section between 400 µm and 79 µm should be removed and placed in a separate labelled sample bag for further processing. The fine fraction < 79 µm should be removed from the bottom and placed in a separate labelled sample bag. The nylon mesh

should be removed from the top and bottom rings and placed in a separate labelled sample bag.
After sieving the 400-79 µm fraction was panned to remove lighter minerals from the sample. The panning method involved adding water to the sample in a small separating pan. Agitating the pan resulted in the denser zircon minerals being concentrated at the bottom of the pan. By gently tilting the smaller pan into a larger water filled container the lighter minerals were washed of the top and into the larger pan. By repeating this process that lighter fraction was reduced to leave only denser minerals in the base of the small pan. The contents of the heavy pan were filtered through filter paper in a funnel. The filter paper with the captured heavy fraction was dried on a hot plate. The lighter mineral contents of the larger pan were filtered through filter paper in a funnel with the filter paper dried overnight in an oven.
When the dense fraction had been dried the magnetic minerals were removed by pouring lines of the dense mineral on a sheet of paper. A magnet covered by a sheet of fine paper was passed over the lines, to remove any magnetic minerals. Any magnetic component was removed and discarded.
Further magnetic processing was conducted using a Frantz Isodynamic Separator Model L-1. The Frantz was initially cleaned to remove sample contaminants. Initially remove the inclined chute by unscrewing from the Frantz. Clean the chute, collection tins, sample funnel and Frantz using compressed air. Ensure that no residual paramagnetic material remains on the electromagnet. Position and screw the chute back into position. The inclined chute of the Frantz was set to an angle of 15 degrees. The amperes setting for the magnet was initially set at 1.5 amps. The coaxial vibrator was set to 10 on the 10 turn potentiometer. The coaxial vibrator and electromagnet are switched on. The sample fraction between 79 and 400 µm was poured into the sample funnel at the top of the separator ramp. The more strongly paramagnetic minerals are separated on the high side of the dividing edge with the more weakly magnetic fraction in the lower side. Both fractions divided are collected and placed in separate labelled bags. Having processed the sample at 1.5 amps the non magnetic fraction was reprocessed through the Frantz at 1.7 amps and then 1.8 amps. The magnetic fractions were placed in labelled bags and the non magnetic fraction was placed in a labelled bag for further processing using heavy liquids.
The heavy liquid separation was performed in a Safe-Tee 200 Fume cupboard. The set up as seen in figure 2, used a funnel that emptied into a 50 ml separating funnel that would drain into a second funnel lined with filter paper. The heavy liquids pass through the filter paper and are collected in a 250 ml conical flask beneath the funnel while the dense mineral concentrate would be collected in the filter paper.
The heavy liquid, methylene iodide, was poured into the funnel that drained into the separating funnel. The separate from the frantz was poured into the separating funnel then stirred and allowed to settle. The separating funnel tap was opened to allow a small flow of liquid from the separating funnel into the heavy liquids bottle beneath. The process of stirring, settling and draining was repeated until the lowest dense fraction of the separating funnel was collected on the filter paper. The filter paper was removed from the collecting funnel and washed with acetone into a liquid disposal bottle. The filter paper with heavy concentrate was placed on a hot plate to dry.
The filter paper was replaced and the remaining contents of the separating funnel were drained through the filter paper into the heavy liquids bottle.

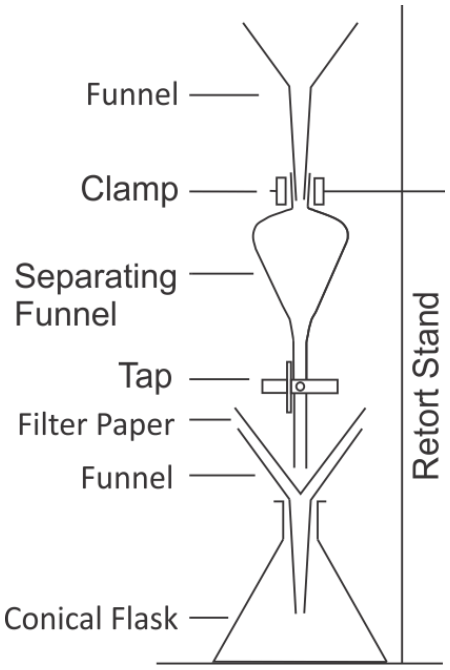


**Supplementary Figure 2 Schematic diagram of Heavy Liquids Separation Apparatus Setup**

Once the separating funnel was drained the bottle of heavy liquids was removed and replaced with a 250 ml conical flask. To inspect for zircon, the dried heavy concentrate was viewed under an Olympus SZ61 optical binocular microscope. Zircons were hand picked to a vial for mounting. If no zircon minerals were observed in the concentrate the process of mineral separation was repeated until sufficient zircons were picked. When sufficient zircons were found the setup was cleaned with acetone draining into the 250 ml conical flask. After cleaning the acetone was disposed of in the liquid disposals container.

The process of mounting zircons required a glass slide to which a strip of double sided tape was placed. A ruler pressed over the tape was used to remove air bubbles before the paper backing was removed from the double sided tape. A strip of clear single sided tape was laid against the double sided tape strip. If air bubbles formed the single sided tape was removed and replaced.

A rubber mould of diameter 25 mm and depth 15 mm was placed onto the tape. The line of the mould was cut into the tape to define the boundary of the mould.

The zircons were poured from the vial into a clean glass petri dish. Under an Olympus SZ61 optical binocular microscope zircons were picked and transferred from the petri dish and affixed to the single sided tape.

When all available zircons up to a number of 150 zircons was reached the picking ceased. The rubber mould was lubricated and realigned with the tape mould outline. Into the mould an epoxy mix of 1:5, epoxy hardener 20-8132-008:epoxy resin 20-8130-032 was poured to a depth of approximately 10 mm. A label for the sample was placed onto the surface of the epoxy mix and submerged. The epoxy mix was allowed to dry for 24 hours. When dry the rubber mould was removed from the epoxy mount. The mount surfaces were manually ground to expose the zircon cores. The surface of the mount was then polished for 10 minutes with a Struers DP-U4 cloth lap with a diamond paste.

Zircon geochronology was undertaken via Laser Ablation Inductively Coupled Mass Spectrometry (LA-ICP-MS) following Payne et al. (2008). The cathodoluminescence and

back Scatter electron imaging of zircon were performed using a Phillips XL40 Scanning Electron Microscope located at Adelaide Microscopy, The University of Adelaide. The cathodoluminesence was used to determine zonation within the mounted zircon.
U/Pb analyses were performed using a NEW Wave UP-213 laser attached to an Agilent 7500cx ICP-MS located at Adelaide Microscopy, The University of Adelaide. The ablation was performed in a helium atmosphere with argon gas added immediately after the cell to aid the transport of material. The spot size for zircon was 30 µm. The spot size was used to target the textural domains present within the grains with maximum signal intensity for the mass spectrometer. The frequency of the laser was 5 Hz and laser output percentage set at 55%, which resulted in average fluence of 2.26 J/cm$^2$ at the ablation site. A single analytical spot consisted of a 40 second gas blank followed by 80 seconds of data acquisition with the laser firing. The measured isotopes and their dwell times are shown in Supplementary Table 12.

**Supplementary Table 12 Measured Isotopes and dwell times for zircon analyses**

| Isotope | Dwell Times |
|---|---|
| $^{204}$Pb | 10 ms |
| $^{206}$Pb | 15 ms |
| $^{207}$Pb | 30 ms |
| $^{238}$U | 15 ms |
| $^{208}$Pb | 10 ms |
| $^{232}$Th | 10ms |

Mass $^{204}$Pb was measured as a monitor of common lead content, and due to the unresolvable isobaric interference of $^{204}$Hg on $^{204}$Pb common lead corrections were not conducted.

The age calculations and mass bias were performed using the GLITTER software with the use of the external primary standards MADel after Payne et al. (2008)and primary zircon standard GJ-1 after
Jackson et al. (2004). The TIMS derived normalization age for MAdel 1 and GJ-1 were assigned an overestimated uncertainty of 1%. Standard bracketing of every 10 unknowns and application of a linear correction was used to correct for instrument drift. The TIMS normalisation data for each isotopic system and standard can be seen in Supplementary Table 13.

**Supplementary Table 13 Published isotopic values of standards, GJ-1 (Jackson et al. 2004), Plešovice (Sláma et al. 2008)**

| Isotopic System | GJ-1 Age (Ma) | Plešovice Age (Ma) |
|---|---|---|
| $^{207}$Pb/$^{206}$Pb | 607.7 ± 4.3 | 339.322 ± 0.25 |
| $^{206}$Pb/$^{238}$U | 600.7 ± 1.1 | 337.13 ± 0.37 |
| $^{207}$Pb/$^{235}$U | 602.0 ± 1.0 | 337.27 ± 0.11 |

Accuracy of the zircon methodology was verified by repeat analysis of Plesovice zircon and an in-house Sri Lankan zircon standard. The weighted average ages for each isotopic system are seen in table 14.

**Supplementary Table 14 Isotopic System Weighted Averages**

| Isotopic System | GJ-1 Age (Ma) (n=62) | Plešovice Age (Ma) (n=15) |
|---|---|---|
| $^{207}Pb/^{206}Pb$ | 612.6 ± 41.1 | 380.1 ± 36.69 |
| $^{206}Pb/^{238}U$ | 599.8 ± 7.9 | 337.72 ± 4.454 |
| $^{207}Pb/^{235}U$ | 602.5 ± 9.2 | 343.95 ± 5.2 |

Due to the unresolvable $^{204}Hg$ on $^{204}Pb$ interference, isotope ratios are presented uncorrected for common lead, with concordia plots generated using Isoplot/Ex 3.71.
Data was rejected based on the presence of common lead using a combination of intensity of the raw $^{204}Pb$ counts, and following this, weighted average $^{207}Pb/^{206}Pb$ age calculations at 2σ are reported.




**Supplementary Figure 3 Photos of muscovite sample outcrop (a) phyllite schist outcrop at sample NZ1306 location, (b) protomylonite outcrop at sample NZ1309 location and (c) mylonite outcrop at sample NZ1312 location**